The Journal of Clinical Endocrinology & Metabolism
URL：https://doi.org/10.1210/clinem/dgac362

Genetic analysis of pheochromocytoma and paraganglioma complicating cyanotic congenital heart disease

Tatsuki Ogasawara[1,2], Yoichi Fujii[1,2], Nobuyuki Kakiuchi[1,3,4], Yusuke Shiozawa[1], Ryuichi Sakamoto[5], Yoshihiro Ogawa[5], Katsuki Ootani[6], Etsuro Ito[6], Tomoaki Tanaka[7], Kenichiro Watanabe[8], Yusaku Yoshida[9], Noriko Kimura[10], Yuichi Shiraishi[11], Kenichi Chiba[11], Hiroko Tanaka[12], Satoru Miyano[12], Seishi Ogawa*[1,2,13]

[1]Department of Pathology and Tumor Biology, Graduate School of Medicine, Kyoto University, Kyoto, Japan
[2]Institute for the Advanced Study of Human Biology (WPI−ASHBi), Kyoto University, Kyoto, Japan
[3]The Hakubi Center for Advanced Research, Kyoto University, Kyoto, Japan
[4]Department of Gastroenterology and Hepatology, Graduate School of Medicine, Kyoto University, Kyoto, Japan
[5]Department of Medicine and Bioregulatory Science, Graduate School of Medical Sciences, Kyushu University, Fukuoka, Japan
[6]Department of Pediatrics, Hirosaki University Graduate School of Medicine, Hirosaki, Japan
[7]Department of Molecular Diagnosis, Graduate School of Medicine, Chiba University, Chiba, Japan
[8]Department of Hematology and Oncology, Shizuoka Children's Hospital, Shizuoka, Japan
[9]Department of Endocrine Surgery, Tokyo Women's Medical University, Tokyo, Japan
[10]Department of Clinical Research Pathology Division, National Hospital Organization Hakodate Hospital, Hakodate, Japan
[11]Division of Genome Analysis Platform Development, National Cancer Center Research Institute, Tokyo, Japan
[12]M&D Data Science Center, Tokyo Medical and Dental University, Tokyo, Japan
[13]Department of Medicine, Center for Hematology and Regenerative Medicine, Karolinska Institute, Stockholm, Sweden

***Corresponding author:**
Seishi Ogawa, MD, PhD
Department of Pathology and Tumor Biology, Graduate School of Medicine, Kyoto University, F-building, Yoshidakonoe-cho, Sakyo-ku, Kyoto, 606-8315, Japan
Phone: +81-75-753-9284; Fax: +81-75-753-9282
E-mail: sogawa-tky@umin.ac.jp
ORCID ID: 0000-0002-7778-5374

Grants and funding sources

This work was supported by the Japan Agency for Medical Research and Development (AMED); the Project for Development of Innovative Research on Cancer Therapeutics (JP15cm0106056 and JP19cm0106501 to S.O.) and the Core Research for Evolutional Science and Technology (CREST) (JP21gm1110011 to S.O.); the Ministry of Education, Culture, Sports, Science and Technology of Japan (MEXT) as ''Priority Issue on Post-K computer'' (hp150265, hp160219, hp170227, hp180198, and hp190158 to S.O.) and ''Program for Promoting Researches on the Supercomputer Fugaku'' (hp200138 and hp210167 to S.O. and S.M.) (this research used computational resources of the K computer/ the supercomputer Fugaku provided by the RIKEN Advanced Institute for Computational Science through the HPCI System Research project); the Japan Society for the Promotion of Science (JSPS); Scientific Research on Innovative Areas (JP15H05909 to S.O. and S.M.; JP15H05912 to S.M.), KAKENHI (JP19H05656 to S.O.); Takeda Science Foundation (S.O.); S.O. is a recipient of JSPS Core-to-Core Program, A. Advanced Research Networks.

Disclosure Summary

The authors have no conflicts of interest to declare.

Abstract

Context:

Pheochromocytoma and paraganglioma (PPGL) may appear as a complication of cyanotic congenital heart disease (CCHD-PPGL) with frequent *EPAS1* mutations, suggesting a close link between *EPAS1* mutations and tissue hypoxia in CCHD-PPGL pathogenesis.

Objective:

Our aim is to further investigate the role of *EPAS1* mutations in the hypoxia-driven mechanism of CCHD-PPGL pathogenesis, particularly focusing on metachronous and/or multifocal CCHD-PPGL tumors.

Methods:

We performed whole exome sequencing (WES) for somatic and germline mutations in 15 PPGL samples from 7 CCHD patients, including 3 patients with metachronous and/or multifocal tumors, together with an adrenal medullary hyperplasia (AMH) sample.

Results:

We detected *EPAS1* mutations in 15 out of 16 PPGL/AMH samples from 7 cases. Conspicuously, all *EPAS1* mutations in each of three cases with multifocal or metachronous tumors were mutually independent and typical examples of parallel evolution, which is suggestive of strong positive selection of *EPAS1*-mutated clones. Compared to 165 TCGA non-CCHD-PPGL samples, CCHD-PPGL/AMH samples were enriched for 11p deletions (13/16) and 2p amplifications (4/16). Of particular note, the multiple metachronous PPGL tumors with additional copy number abnormalities developed 18-23 years after the resolution of hypoxemia, suggesting that CCHD-induced hypoxic environments are critical for positive selection of *EPAS1* mutants in early life, but may no longer be required for development of PPGL in later life.

Conclusions:

Our results highlight a key role of activated HIF2α due to mutated *EPAS1* in positive selection under hypoxic environments, although hypoxemia itself may not necessarily be required for the *EPAS1*-mutated clones to progress to PPGL.

Keywords:

Pheochromocytoma, paraganglioma, cyanotic congenital heart disease, whole exome sequencing, clonal selection, HIF2α

Introduction

Pheochromocytoma and paraganglioma (PPGL) are catecholamine-producing tumors originating from chromaffin cells occurring in adrenal medulla and extra-adrenal paraganglia. Most frequently presented as an isolated tumor, PPGL might also be found in association with hereditary syndromes such as multiple endocrine neoplasia type 2 (MEN2), neurofibromatosis type 1 (NF1), or von Hippel-Lindau syndrome (VHL). During the past three decades, understanding of the molecular mechanism of PPGL has been dramatically improved through the identification of germline variants involving more than 15 PPGL susceptibility genes (1,2). Conspicuously, the majority of these genes, including *VHL*, *SDHA*, *SDHB*, *SDHC*, *SDHD*, *SDHAF2*, *EGLN1*, *FH*, *MDH2* and *EPAS1,* are implicated in a common signaling pathway that activates hypoxia-inducible factors (3), suggesting the role of hypoxic environments in PPGL pathogenesis.

Besides germline predisposition, the role of hypoxic environment has also been discussed in the pathogenesis of PPGL based on the report of a significantly elevated prevalence of head and neck paraganglioma among those who live at high altitude (4). Also supporting this is an observation that patients with cyanotic congenital heart disease (CCHD) who suffer from chronic hypoxia have an increased risk of developing PPGL (CCHD-PPGL), which frequently presents itself as multicentric and/or metachronous tumors (5,6). Although previous studies have implicated the activated HIF pathway in PPGL pathogenesis (3,7-9), the molecular link between hypoxic environment itself and PPGL had been poorly understood. In this regard, a recent report of somatic gain-of-function mutations of *EPAS1* encoding HIF2α in four out of five CCHD-PPGL patients shed new light on CCHD-PPGL pathogenesis, in that they provided a direct explanation of the activated HIF pathway (10), where the somatic *EPAS1* mutations positively selected under hypoxic environments are responsible for the activated HIF pathway. However, due to the limited number of cases and the lack of unbiased analysis, genetic features of CCHD-PPGL are still to be fully elucidated in terms of the role of *EPAS1* mutations in early selection and that of mutational burden and copy number alterations in disease progression.

In this study, to elucidate the molecular pathogenesis of CCHD-PPGL, particularly the role of hypoxic environments, we performed whole exome sequencing (WES) of 16 CCHD-PPGL samples from seven patients, including three with multicentric tumors, and compared mutational profiles of CCHD-PPGL with those of CCHD-unrelated PPGL from The Cancer Genome Atlas (TCGA) project (11).

Materials and Methods

Patients and materials

We enrolled seven patients who were diagnosed with pheochromocytoma or paraganglioma (PPGL) complicated by cyanotic congenital heart disease (CCHD) and were underwent surgical resection or autopsy at Chiba University Hospital (n=1), Kyushu University Hospital (n=1), Hirosaki University Hospital (n=2), Shizuoka Children's Hospital (n=2) and Tokyo Women's Medical University Hospital (n=1). Written informed consent for this research was obtained from all alive patients. This study was approved by the ethics committee of the Graduate School of Medicine, Kyoto University, and other participating institutes.

We obtained a total of 15 PPGL and paired germline samples from surgical/autopsy specimens or peripheral blood in seven patients. In Case 3, an additional sample was collected from adrenal medullary hyperplasia (AMH) **(Supplementary Figure 1)** (12), which is, in most cases, associated with known hereditary PPGL syndromes and thought to represent a precursor lesion of pheochromocytoma (13-15). Among these, 10 PPGL/AMH and two germline samples were obtained from formalin fixed paraffin embedded (FFPE) tissues using macro-dissection, while six PPGL and five germline samples were derived from fresh frozen tissues and peripheral blood, respectively. Genomic DNA was extracted using GeneRead DNA FFPE Kit (QIAGEN) from FFPE tissues and DNeasy Blood & Tissue Kit (QIAGEN) or Gentra Puregene Blood Kit (QIAGEN) from fresh frozen tissues. A full description of the samples is provided in **Supplementary Table 1** (12).

External dataset

We obtained public sequencing data of PPGLs from TCGA cohort (11). Bam files of whole exome sequencing (WES) data were downloaded from the TCGA Data Portal (https://portal.gdc.cancer.gov/).

Whole exome sequencing and somatic mutation detection

All tumors and matched germline samples were subjected to WES. WES libraries were prepared using xGen Exome Research Panel v2 (IDT), followed by sequencing of enriched exon fragments on a DNBSEQ-G400RS (MGI) in 100 or 150-bp paired-end mode with an average depth of 131x (110x-200x) and 156x (117x-309x) for tumor and germline DNA, respectively. Sequence alignment and mutation calling were performed using Genomon2 pipelines (https://genomon.readthedocs.io/ja/latest/), as previously reported (16,17). Briefly, sequencing reads were aligned to the human genome reference (GRCh37) using Burrows-Wheeler Aligner, version 0.7.8 with default parameter settings. PCR duplicates were eliminated using biobambam version 0.0.191 (https://github.com/gt1/biobambam). Somatic mutations were detected by eliminating polymorphisms and sequencing errors. To achieve this, Genomon2 first discards any of low-quality, unreliable reads and variants according to the following criteria: (i) mapping

quality < 20, (ii) base call quality < 15. Variants were further filtered by the following criteria: (iii) both of tumor and normal depths ≥8, (iv) number of variant reads in tumor ≥ 4, (v) number of variant reads in normal ≤ 1, (vi) variant allele frequencies (VAFs) in tumor ≥ 0.05, (vii) VAFs in germline control ≤ 0.02, (viii) Fisher's exact test $P < 10^{-1}$, (ix) presenting in bidirectional reads. To select variants that were observed at significantly higher VAFs than expected for errors, we used the following criteria: (x) $P \leq 10^{-4}$, for which significance is evaluated by EBcall algorithm (18) on the basis of an empirical distribution of VAFs as determined using WES data of non-paired germline samples (n=15-20). The candidate mutations were subjected to visual inspection on the Integrative Genomics Viewer (19), to further eliminate sequencing errors.

Germline mutation analysis

Bam files from exome sequencing of germline DNA were analyzed to call germline variants according to the following criteria : (i) variants in known PPGL susceptibility genes, (ii) VAFs in germline samples ≥ 0.2 (20), (iii) minor allele frequencies in ESP, the 1000 genomes project, ExAC and HGVD <0.001. Truncating mutations (nonsense mutations or frameshift indels) in tumor-suppressor genes and missense and splice site mutations registered as "pathogenic" or "likely pathogenic" in ClinVar (https://www.ncbi.nlm.nih.gov/clinvar/) (21) were considered as pathogenic variants in this study.

Analysis of somatic mosaicism of EPAS1 mutants

Deep-sequencing analysis of germline DNA from the seven CCHD patients, obtained from peripheral blood (n=5), lymph node (n=1) and liver tissue (n=1), was performed for detection of mosaic *EPAS1* variants. Mosaic *EPAS1* variants were called according to the following criteria: (i) identical *EPAS1* variants that were found in tumors in paired germline DNA, (ii) VAFs in the germline samples were more than those found in unrelated germline samples from other CCHD cases, (iii) VAFs in the germline samples were more than background error levels calculated based on the VAFs of other 141 *EPAS1* variants observed in the germline samples that were thought to be artifacts.

Validation of somatic EPAS1 mutations

PCR−based deep sequencing was performed for validation of *EPAS1* mutations detected in WES (22). Mutations were considered to be validated when (i) Sequencing depths ≥ 500 in both tumor and paired germline samples; (ii) VAFs in the tumor samples were 5 times higher than those in the corresponding germline samples; (iii) VAFs in the tumor samples ≥ 0.01 (16,17). This allowed us to validate all *EPAS1* mutations. The results of validation sequencing are summarized in **Supplementary Table 3** (12)**.**

Analysis of copy number alterations

Copy number alterations (CNAs) were evaluated from WES data using our in-house pipeline, 'CNACS' (https://github.com/papaemmelab/toil_cnacs) (23). The fractions of genomic regions with CNAs were compared between PPGLs with and without CCHD. The overall chromosomal instability of each sample was quantified as weighted genome instability index (24): the percentage of aberrant genomic material relative to the ploidy for each chromosome was calculated separately, and the mean percentage of aberrations was then calculated across all 22 chromosomes. In this analysis, we defined an arm-level event as any event spanning more than 50% of a chromosome arm.

Immunohistochemistry

FFPE sections of PPGL/AMH from Case3 were stained with commercially available mouse monoclonal Chromogranin A antibody (RRID: AB_2081135, DAK-A3, DAKO, Santa Clara, CA, USA; 1:100 dilution, 32min) on an automatic Ventana Benchmark Ultra System (Ventana Medical Systems, Tuscon, AZ, USA) using Ultraview diaminobenzidine (DAB) detection system. Results were reviewed by a pathologist (N.K.).

Statistical analysis

Statistical analyses were performed using R, version 4.0.2. All *P* values were calculated by two-sided analysis. Fisher's exact test or Mann–Whitney *U* test was used for group comparisons. Multiple testing was corrected for by the method proposed by Benjamini-Hochberg, in which $q < 0.1$ was considered to be significant.

Results

Clinical characteristics of CCHD-PPGL patients

Clinical features of the seven CCHD-PPGL cases are summarized in **Table 1** and **Supplementary Table 1** (12). The patients had a median age of 26 years (range 18–46 years) at initial diagnosis of PPGL/AMH with a median cumulative duration of cyanosis of 26 years (range 12-46 years). The median oxygen saturation at PPGL diagnosis was 80% (range 50-95%). Four patients had a single tumor, while the remining three (Case 1-3) presented with multifocal tumors. None of the 7 patients had symptoms of somatostatinoma suggestive of somatic mosaicism of *EPAS1* mutants (25-27), although three patients had polycythemia (Case 1, 3, 6), which was most likely caused by chronic hypoxemia (28). During the follow-up period after PPGL diagnosis, one patient (Case 5) experienced metastasis and two (Case 3 and 5) died of progressive heart failure.

Somatic mutations and copy number alterations in CCHD-PPGL

With a median depth of 136 (range 110-308), WES in 15 PPGL and 1 AMH (Case 3) samples from 7 patients identified 98 single-nucleotide variants (SNVs) and six insertion-deletions (indels) **(Supplementary Table 2)** (12). With a median of 1.5 synonymous and 4 nonsynonymous

mutations per sample, CCHD-PPGL/AMH samples showed a low mutation burden of 0.18 mutations/Mb, which is comparable to that of non-CCHD PPGL **(Fig. 1a)**. As is the case with many types of cancers, these somatic mutations were enriched for C>T transitions **(Fig. 1b)** (29-31). Recurrent mutations were observed only in *EPAS1* encoding HIF2α. *EPAS1* was mutated in 15 out of 16 CCHD-PPGL samples (94%) **(Fig. 1a)**, where all mutations were validated through targeted amplicon sequencing **(Supplementary Table 3)** (12). All mutations were found in the oxygen-dependent degradation domain of HIF2α, most frequently affecting p.P531 **(Fig. 1c)**, which has been reported to enhance HIF2α stability and promote tumor growth in vivo (32). None of these cases had germline mutations in known PPGL predisposition genes, including *VHL*, *SDHA*, *SDHB*, *SDHC*, *SDHD*, *SDHAF2*, *EGLN1*, *FH, MDH2, RET, NF1, MAX* and *TMEM127*. Given the previous reports of somatic mosaicism of *EPAS1* mutations in the cases with multifocal PPGL (25,26,33), we assessed whether or not these *EPAS1* mutations were derived from somatic mosaicism based on the targeted sequencing of germline DNA samples from peripheral blood (n=5), lymph node (n=1) and liver tissue (n=1). With a mean depth of >1,000,000×, targeted sequencing did detect the *EPAS1* variants identical to those found in tumors in paired germline DNA. However, with only small numbers of supportive reads for these variants, their VAFs (<0.23%) were substantially lower than those reported for mosaic *EPAS1* mutations (2-9%) (26,33) **(Supplementary Fig. 1)** (12). In addition, the majority of these *EPAS1* variants had lower VAFs than those found in unrelated germline samples from other CCHD cases and therefore, were indistinguishable from the background error levels. Thus, no evidence suggests the presence of somatic mosaicism carrying *EPAS1* mutations found in the tumor samples, although we did not examine other germline tissues.

In sequencing-based analysis of chromosomal copy numbers (23), copy number alterations (CNAs) were detected in all 16 CCHD-PPGL/AMH samples and most frequently affected 11p (deletion) (n=13), followed by 1p (deletion) (n=8) and 3p (deletion) (n=5) **(Fig. 1a)**. Although some samples showed extensive CNAs, chromosomal instability, as determined by weighted genome instability index (24), remained moderate in the majority of cases (median 0.06).

Comparison of genetic and clinical features between CCHD-PPGL and non-CCHD PPGL

To delineate the genetic features of CCHD-PPGL, we used 173 PPGL cases from the TCGA project (TCGA-PPGL) as a non-CCDH-PPGL cohort and compared their genetic and clinical profiles with that in our CCHD-PPGL cases based on the publicly available WES data. For this purpose, we newly called pathogenic variants and CNAs from TCGA WES data using the identical pipeline that was used to analyze our CCHD-PPGL data. We identified pathogenic germline variants in known PPGL-predisposing genes in 44 cases (25%), while somatic mutations in known driver genes were detected in 64 cases (37%) **(Fig. 2a)**. Among these, 37 variants in 37 cases (21%) affected hypoxia-related genes, including *SDHB*, *SDHD*, *VHL*, *EGLN1*, *IDH1* and *EPAS1,* of which *EPAS1* mutations

were found in 8 cases (5%). Because *EPAS1*-mutated PPGL in the TCGA-PPGL cases could be associated with CCHD, in the following analyses, comparisons were made by excluding *EPAS1*-mutated PPGL cases from the TCGA "non-CCHD-PPGL" cases.

CNAs were common and found in virtually all cases with non-CCHD-PPGL cases (96%), where 1p (74%) and 3q (61%) were most frequently affected **(Fig. 2a)**. There were no significant differences in the affected chromosomal segments between CCHD-PPGL and non-CCHD-PPGL except for 11p deletions and 2p amplifications, which were significantly more frequent in CCHD-PPGL (81% vs. 28%, 25% vs. 5%), as well as 3q deletions which were less common in CCHD-PPGL (25% vs. 56%) **(Fig. 2b, c)**. Of note, when focusing on the cases having mutations in hypoxia-related genes in non-CCHD-PPGL, there were no significant deference in frequencies of 11p deletion and 2p amplification between CCHD-PPGL and non-CCHD-PPGL (81% vs. 52%, 25% vs. 14%), whereas deletions in 3q were less common in CCHD-PPGL cases (25% vs. 72%) **(Fig. 2b, d)**.

Comparing clinical parameters between patients with CCHD-PPGL and non-CCHD-PPGL, CCHD-PPGL cases were associated with a younger onset (median of 26 yr vs. 46 yr) and likely to present with multicentric (43% vs. 6%) and extra-adrenal tumors (86% vs. 17%) as previously reported (6) **(Supplementary Table 4)** (12). When focusing on non-CCHD-PPGL patients with hypoxia-related gene mutations, most of the cases (86%) harbored a germline mutation in either *VHL*, *SDHB*, *SDHD* or *EGLN1*, they were likely to be young at PPGL diagnosis (median 39 yr vs. 46 yr) and show multifocal extra-adrenal tumors (24% vs. 2%) as compared with those without mutations in hypoxia related genes, whereas patients with CCHD-PPGL were even much younger at PPGL diagnosis than those with non-CCHD-PPGL patients harboring hypoxia-related gene mutations (median 26 yr vs. 39 yr) **(Table 2)**.

Independent EPAS1 mutations in multifocal CCHD-PPGLs

Three patients had multifocal PPGL tumors (Cases 1-3). In Case 1, two retroperitoneal paragangliomas (PGLs) and a pheochromocytoma (PCC) were diagnosed after a 26 years' exposure to severe hypoxia **(Fig. 3a)**. Case 2 developed a PCC at the age of 19 (not available), followed by each 3 retroperitoneal PGL tumors at the age of 30 and 35, even though hypoxemia was resolved at the age of 12 by the Fontan procedure **(Fig. 3b)**. In Case 3, who died of progressive heart failure after suffering from severe hypoxemia for 32 years, a microscopic PGL in the bladder in addition to a large PCC and an AMH in the left and right adrenal gland, respectively were pathologically diagnosed at autopsy **(Fig. 3c)**. In the right adrenal gland, the medulla expanded to comprise more than two-thirds of the gland thickness in the absence of cortical atrophy, supporting the diagnosis of AMH **(Supplementary Fig. 2)** (12).

We investigated the clonal origins of multifocal PPGLs found in these cases, by testing whether they have an independent or common clonal origin. Each PPGL/AMH sample had 3-12 somatic mutations, including an *EPAS1* mutation in most samples, but none of them were shared across

different samples, suggesting independent clonal origins **(Fig. 3a, b, c)**. Meanwhile, all samples harbored some CNAs, among which 11p deletions were found in all multifocal/metachronous tumors from Case 1 and 2 and an AMH from Case 3 **(Fig. 3d)**, suggesting their role in CCHD-PPGL development.

Discussion

Approximately 15% of PPGL patients present with multicentric and/or metachronous extra-adrenal tumors (34). The majority of these cases are explained by the presence of pathogenic germline variants affecting hypoxia related genes or in rare cases, somatic mosaicism of these mutations, i.e., as exemplified by the Pacak-Zhuang syndrome caused by a mosaicism of an activating *EPAS1*-mutation (25-27). These multicentric and/or metachronous PPGL tumors typically show an early onset, in which a common clonal origin has rationally been proposed with second-hit events being acquired during embryogenic migration of neural crest precursors (35). However, this may not necessarily be the case with CCHD-PPGL. CCHD-PPGL is another condition in which frequent multicentric and/or metachronous tumors are observed. A key finding on CCHD-PPGL of recent years is a highly frequent *EPAS1* mutations encoding HIF2α, suggesting that CCHD-PPGL tumors are selected in hypoxic environment by means of an activating HIF2α activity caused by *EPAS1* mutations, although *EPAS1* mutations have not been analyzed in multicentric/metachronous tumors (10). The current study not only confirmed the previous finding of frequent *EPAS1* mutations in CCHD-PPGL cases (15/16 tumors), but also revealed that except for one *EPAS1*-negative tumors, all multicentric/metachronous tumors in three cases harbored independent *EPAS1* activating mutations indicative of parallel evolution (36,37). Given that no germline or mosaic *EPAS1* variants were detected, these findings unequivocally confirm that activating *EPAS1* mutated chromaffin cells are strongly positively selected in CCHD cases, most likely due to tissue hypoxia. Sensitivity of chromaffin cells to hypoxia has been functionally supported by an observation that rat pheochromocytoma PC12 cells derived from chromaffin cells of the adrenal medulla undergo apoptosis when exposed to hypoxia (38). Moreover, *EPAS1*-mutated PPGL showed increased expressions of HIF-responsive genes encoding VEGF-A, cyclin D1 and IGF2 (32), which might confer an anti-apoptotic and proliferative advantage to *EPAS1*-mutated chromaffin cells under hypoxic conditions (39-42). The strong positive selection of *EPAS1* mutations under hypoxic conditions in CCHD-PPGL further suggests a critical role of hypoxic environments in non-CCHD-PPGL with *EPAS1* mutations, particularly in those with multicentric and/or metachronous tumors, even when there are no clear manifestations suggestive of tissue hypoxia. In fact, Ben Aim et al., reported two independent non-CCHD-PPGL tumors harboring different *EPAS1* mutations in a patient with non-symptomatic heterozygous hemoglobin C disease, which abnormal hemoglobin C is implicated in tissue hypoxia (43). Somatic *EPAS1* mutations were also reported in 8 of 173 TCGA PPGL cases, of which 2 had

multicentric tumors. Unfortunately, however, no clinical information was available with regard to the possible complications suggesting the presence of hypoxic environments. On the basis of the above discussion, chronic tissue hypoxia may also be involved in the development of PPGL with somatic mutations in other hypoxia-associated genes, such as *VHL*, in the early stages of PPGL tumorigenesis. However, currently there is no evidence suggesting the involvement of mutations in any hypoxia-related gene other than *EPAS1* in CCHD-PPGL cases, although the number of CCHD-PPGL cases thus far analyzed for mutations is still limited.

Another important finding in our study is the observation in Case 2 who developed PPGL tumors at the age of 19, 30, and 35, long after his hypoxemia was corrected at the age of 12, which provides unique insight into the evolution of CCHD-PPGL and the role of hypoxemia therein. Given that the selection of *EPAS1* mutated cells depend on the hypoxic echo system imposed by CCHD, the *EPAS1*-mutated ancestors of these metachronous PPGL tumors were thought to originally be selected 7-23 years before the diagnosis through the acquisition of *EPAS1* mutations and contribute to the development of PPGL in the later life, even after the hypoxemia by which they were selected was corrected. This suggests that *EPAS1*-mutated cells may no longer require hypoxia for their progression to PPGL, even though the initial selection of *EPAS1* mutated cells depends on the presence of tissue hypoxia. A possible explanation would be that *EPAS1* mutations, which are more efficiently selected in the presence of hypoxemia, can still confer a selective advantage in non-cyanotic conditions. Alternatively, there were many *EPAS1*-mutated clones selected by hypoxemia, of which only those clones that acquired additional genetic hits were further selected to develop PPGL, after hypoxemia was corrected **(Fig. 3e)**. Among the candidates of those genetic hits are 11p deletion and 2p amplification, which were significantly enriched in CCHD-PPGL compared to non-CCHD-PPGL and might contribute to the development of *EPAS1*-mutated PPGL. Of note in this regard, low tissue oxygen pressure has long been implicated in genomic instability (44-46). Thus, chronic tissue hypoxia might promote these secondary genetic hits to take place in chromaffin cells. Among these secondary lesions, 2p amplification involved the *EPAS1* locus in common, which might contribute to an augmented HIF2α function (47), although the underlying molecular basis of 11p deletion in the pathogenesis of PPGL associated with hypoxia signaling is still elusive and needs further studies. Of interest, the frequencies of 11p deletion and 2p amplification were not significantly different between CCHD-PPGL and non-CCHD-PPGL with hypoxia-related genes, suggesting that these CNAs can confer a growth advantage on PPGLs associated with hypoxia signaling.

Finally, even though CCHD is a relatively rare disease, occurring only in 1 in 500 births (0.2%) (48), as many as 4% of these CCHD cases will develop CCHD-PPGL (49). Given that this relatively high frequency of PPGL complication in a rare disease, we would recommend an active screening of the complication in all CCHD cases, because hypertension and tachycardia due to

hypercathecholaminemia have a harmful effect on CCHD and may exacerbate the underlying heart failure. Of note in this regard, the diagnosis of PPGL in CCHD patients tends to be delayed because the symptoms of PPGL overlap with those of heart disease, underscoring the importance of early diagnosis by an active screening. Among 7 CCHD-PPGL cases in our cohort, two died of progressive heart failure. Given that heart failure is the major cause of mortality in patients with PPGL, the complication of CCHD could negatively affect the mortality of CCHD-PPGL patients. However, the number of observations in CCHD-PPGL is still too small to evaluate this, which should be addressed in future studies.

In conclusion, our finding of parallel evolution of multiple *EPAS1*-mutated tumors in three CCHD patients with multifocal PPGLs suggests that *EPAS1*-mutated clones are strongly selected in chromaffin tissues at an early stage of tumorigenesis in a chronic hypoxia-dependent manner, although hypoxia itself might no longer be required for the development of PPGL tumors once they acquired an *EPAS1* mutation. 11p deletion and 2p amplification, which were significantly enriched in CCHD-PPGL compared to non-CCHD-PPGL, might contribute to the development of *EPAS1*-mutated PPGL.

Acknowledgement

We thank Takeshi Shirahari and Atsuko Ryu for technical assistance. We also thank Masatoshi Ogata, Masanori Fujimoto, Noriko Kato and Kaoru Ogawa for collecting samples.

Author contributions

T.O., Y. F. and S.O. designed the study. R.S., Y.O., K.O., E.I., T.T., K.W. and Y.Y. provided specimens. N.K. performed pathological assessment. T.O. performed sample preparation. N.K. performed sequencing. T.O., Y.F., N.K., Y. Shiozawa, Y. Shiraishi, K.C., H.T., and S.M performed bioinformatics analysis. T.O., Y.F., N.K. and S.O. prepared the manuscript.

Abbreviations

PPGL, pheochromocytoma and paraganglioma; CCHD, cyanotic congenital heart disease; WES, whole exome sequencing; AMH, adrenal medullary hyperplasia; TCGA, The Cancer Genome Atlas project; HIF, hypoxia-inducible factor; CNA, copy number alteration; PCC, pheochromocytoma; PGL, paraganglioma.

Data Availability

The data supporting the findings presented in this study are available from the corresponding authors upon reasonable request.

References

1. Toledo RA, Burnichon N, Cascon A, Benn DE, Bayley JP, Welander J, Tops CM, Firth H, Dwight T, Ercolino T, Mannelli M, Opocher G, Clifton-Bligh R, Gimm O, Maher ER, Robledo M, Gimenez-Roqueplo AP, Dahia PL. Consensus Statement on next-generation-sequencing-based diagnostic testing of hereditary phaeochromocytomas and paragangliomas. *Nat Rev Endocrinol*. 2017;13(4):233-247.
2. Dahia PL. Pheochromocytoma and paraganglioma pathogenesis: learning from genetic heterogeneity. *Nat Rev Cancer*. 2014;14(2):108-119.
3. Dahia PLM, Toledo RA. Recognizing hypoxia in phaeochromocytomas and paragangliomas. *Nat Rev Endocrinol*. 2020;16(4):191-192.
4. Saldana MJ, Salem LE, Travezan R. High altitude hypoxia and chemodectomas. *Hum Pathol*. 1973;4(2):251-263.
5. Folger GM, Jr., Roberts WC, Mehrizi A, Shah KD, Glancy DL, Carpenter CC, Esterly JR. CYANOTIC MALFORMATIONS OF THE HEART WITH PHEOCHROMOCYTOMA. A REPORT OF FIVE CASES. *Circulation*. 1964;29:750-757.
6. Opotowsky AR, Moko LE, Ginns J, Rosenbaum M, Greutmann M, Aboulhosn J, Hageman A, Kim Y, Deng LX, Grewal J, Zaidi AN, Almansoori G, Oechslin E, Earing M, Landzberg MJ, Singh MN, Wu F, Vaidya A. Pheochromocytoma and paraganglioma in cyanotic congenital heart disease. *J Clin Endocrinol Metab*. 2015;100(4):1325-1334.
7. Dahia PL, Ross KN, Wright ME, Hayashida CY, Santagata S, Barontini M, Kung AL, Sanso G, Powers JF, Tischler AS, Hodin R, Heitritter S, Moore F, Dluhy R, Sosa JA, Ocal IT, Benn DE, Marsh DJ, Robinson BG, Schneider K, Garber J, Arum SM, Korbonits M, Grossman A, Pigny P, Toledo SP, Nosé V, Li C, Stiles CD. A HIF1alpha regulatory loop links hypoxia and mitochondrial signals in pheochromocytomas. *PLoS Genet*. 2005;1(1):72-80.
8. Jochmanová I, Yang C, Zhuang Z, Pacak K. Hypoxia-inducible factor signaling in pheochromocytoma: turning the rudder in the right direction. *J Natl Cancer Inst*. 2013;105(17):1270-1283.
9. Jochmanová I, Zelinka T, Widimský J, Jr., Pacak K. HIF signaling pathway in pheochromocytoma and other neuroendocrine tumors. *Physiol Res*. 2014;63(Suppl 2):S251-262.
10. Vaidya A, Flores SK, Cheng ZM, Nicolas M, Deng Y, Opotowsky AR, Lourenço DM, Jr., Barletta JA, Rana HQ, Pereira MA, Toledo RA, Dahia PLM. EPAS1 Mutations and Paragangliomas in Cyanotic Congenital Heart Disease. *N Engl J Med*. 2018;378(13):1259-1261.
11. Fishbein L, Leshchiner I, Walter V, Danilova L, Robertson AG, Johnson AR, Lichtenberg TM, Murray BA, Ghayee HK, Else T, Ling S, Jefferys SR, de Cubas AA, Wenz B, Korpershoek

E, Amelio AL, Makowski L, Rathmell WK, Gimenez-Roqueplo AP, Giordano TJ, Asa SL, Tischler AS, Pacak K, Nathanson KL, Wilkerson MD. Comprehensive Molecular Characterization of Pheochromocytoma and Paraganglioma. *Cancer Cell*. 2017;31(2):181-193.

12. Ogasawara T, Fujii Y, Kakiuchi N, Shiozawa Y, Sakamoto R, Ogawa Y, K. O, Ito E, Tanaka T, Watanabe K, Yoshida Y, Kimura N, Shiraishi Y, Chiba K, Tanaka H, Miyano S, Ogawa S. Genetic analysis of pheochromocytoma and paraganglioma complicating cyanotic congenital heart disease. Dataset. Zenodo. Posted May 24, 2022. Available at: https://doi.org/10.5281/zenodo.6577551.
13. Korpershoek E, Petri BJ, Post E, van Eijck CH, Oldenburg RA, Belt EJ, de Herder WW, de Krijger RR, Dinjens WN. Adrenal medullary hyperplasia is a precursor lesion for pheochromocytoma in MEN2 syndrome. *Neoplasia*. 2014;16(10):868-873.
14. Carney JA, Sizemore GW, Sheps SG. Adrenal medullary disease in multiple endocrine neoplasia, type 2: pheochromocytoma and its precursors. *Am J Clin Pathol*. 1976;66(2):279-290.
15. van Nederveen FH, de Krijger RR. Precursor lesions of the adrenal gland. *Pathobiology*. 2007;74(5):285-290.
16. Yokoyama A, Kakiuchi N, Yoshizato T, Nannya Y, Suzuki H, Takeuchi Y, Shiozawa Y, Sato Y, Aoki K, Kim SK, Fujii Y, Yoshida K, Kataoka K, Nakagawa MM, Inoue Y, Hirano T, Shiraishi Y, Chiba K, Tanaka H, Sanada M, Nishikawa Y, Amanuma Y, Ohashi S, Aoyama I, Horimatsu T, Miyamoto S, Tsunoda S, Sakai Y, Narahara M, Brown JB, Sato Y, Sawada G, Mimori K, Minamiguchi S, Haga H, Seno H, Miyano S, Makishima H, Muto M, Ogawa S. Age-related remodelling of oesophageal epithelia by mutated cancer drivers. *Nature*. 2019;565(7739):312-317.
17. Kakiuchi N, Yoshida K, Uchino M, Kihara T, Akaki K, Inoue Y, Kawada K, Nagayama S, Yokoyama A, Yamamoto S, Matsuura M, Horimatsu T, Hirano T, Goto N, Takeuchi Y, Ochi Y, Shiozawa Y, Kogure Y, Watatani Y, Fujii Y, Kim SK, Kon A, Kataoka K, Yoshizato T, Nakagawa MM, Yoda A, Nanya Y, Makishima H, Shiraishi Y, Chiba K, Tanaka H, Sanada M, Sugihara E, Sato TA, Maruyama T, Miyoshi H, Taketo MM, Oishi J, Inagaki R, Ueda Y, Okamoto S, Okajima H, Sakai Y, Sakurai T, Haga H, Hirota S, Ikeuchi H, Nakase H, Marusawa H, Chiba T, Takeuchi O, Miyano S, Seno H, Ogawa S. Frequent mutations that converge on the NFKBIZ pathway in ulcerative colitis. *Nature*. 2020;577(7789):260-265.
18. Shiraishi Y, Sato Y, Chiba K, Okuno Y, Nagata Y, Yoshida K, Shiba N, Hayashi Y, Kume H, Homma Y, Sanada M, Ogawa S, Miyano S. An empirical Bayesian framework for somatic mutation detection from cancer genome sequencing data. *Nucleic Acids Res*. 2013;41(7):e89.

19. Thorvaldsdóttir H, Robinson JT, Mesirov JP. Integrative Genomics Viewer (IGV): high-performance genomics data visualization and exploration. *Brief Bioinform*. 2013;14(2):178-192.
20. Inagaki-Kawata Y, Yoshida K, Kawaguchi-Sakita N, Kawashima M, Nishimura T, Senda N, Shiozawa Y, Takeuchi Y, Inoue Y, Sato-Otsubo A, Fujii Y, Nannya Y, Suzuki E, Takada M, Tanaka H, Shiraishi Y, Chiba K, Kataoka Y, Torii M, Yoshibayashi H, Yamagami K, Okamura R, Moriguchi Y, Kato H, Tsuyuki S, Yamauchi A, Suwa H, Inamoto T, Miyano S, Ogawa S, Toi M. Genetic and clinical landscape of breast cancers with germline BRCA1/2 variants. *Commun Biol*. 2020;3(1):578.
21. Landrum MJ, Lee JM, Riley GR, Jang W, Rubinstein WS, Church DM, Maglott DR. ClinVar: public archive of relationships among sequence variation and human phenotype. *Nucleic Acids Res*. 2014;42(Database issue):D980-985.
22. Suzuki H, Aoki K, Chiba K, Sato Y, Shiozawa Y, Shiraishi Y, Shimamura T, Niida A, Motomura K, Ohka F, Yamamoto T, Tanahashi K, Ranjit M, Wakabayashi T, Yoshizato T, Kataoka K, Yoshida K, Nagata Y, Sato-Otsubo A, Tanaka H, Sanada M, Kondo Y, Nakamura H, Mizoguchi M, Abe T, Muragaki Y, Watanabe R, Ito I, Miyano S, Natsume A, Ogawa S. Mutational landscape and clonal architecture in grade II and III gliomas. *Nat Genet*. 2015;47(5):458-468.
23. Yoshizato T, Nannya Y, Atsuta Y, Shiozawa Y, Iijima-Yamashita Y, Yoshida K, Shiraishi Y, Suzuki H, Nagata Y, Sato Y, Kakiuchi N, Matsuo K, Onizuka M, Kataoka K, Chiba K, Tanaka H, Ueno H, Nakagawa MM, Przychodzen B, Haferlach C, Kern W, Aoki K, Itonaga H, Kanda Y, Sekeres MA, Maciejewski JP, Haferlach T, Miyazaki Y, Horibe K, Sanada M, Miyano S, Makishima H, Ogawa S. Genetic abnormalities in myelodysplasia and secondary acute myeloid leukemia: impact on outcome of stem cell transplantation. *Blood*. 2017;129(17):2347-2358.
24. Burrell RA, McClelland SE, Endesfelder D, Groth P, Weller MC, Shaikh N, Domingo E, Kanu N, Dewhurst SM, Gronroos E, Chew SK, Rowan AJ, Schenk A, Sheffer M, Howell M, Kschischo M, Behrens A, Helleday T, Bartek J, Tomlinson IP, Swanton C. Replication stress links structural and numerical cancer chromosomal instability. *Nature*. 2013;494(7438):492-496.
25. Zhuang Z, Yang C, Lorenzo F, Merino M, Fojo T, Kebebew E, Popovic V, Stratakis CA, Prchal JT, Pacak K. Somatic HIF2A gain-of-function mutations in paraganglioma with polycythemia. *N Engl J Med*. 2012;367(10):922-930.
26. Buffet A, Smati S, Mansuy L, Ménara M, Lebras M, Heymann MF, Simian C, Favier J, Murat A, Cariou B, Gimenez-Roqueplo AP. Mosaicism in HIF2A-related polycythemia-paraganglioma syndrome. *J Clin Endocrinol Metab*. 2014;99(2):E369-373.

27. Pacak K, Jochmanova I, Prodanov T, Yang C, Merino MJ, Fojo T, Prchal JT, Tischler AS, Lechan RM, Zhuang Z. New syndrome of paraganglioma and somatostatinoma associated with polycythemia. *J Clin Oncol*. 2013;31(13):1690-1698.
28. Zabala LM, Guzzetta NA. Cyanotic congenital heart disease (CCHD): focus on hypoxemia, secondary erythrocytosis, and coagulation alterations. *Paediatr Anaesth*. 2015;25(10):981-989.
29. Alexandrov LB, Nik-Zainal S, Wedge DC, Aparicio SA, Behjati S, Biankin AV, Bignell GR, Bolli N, Borg A, Børresen-Dale AL, Boyault S, Burkhardt B, Butler AP, Caldas C, Davies HR, Desmedt C, Eils R, Eyfjörd JE, Foekens JA, Greaves M, Hosoda F, Hutter B, Ilicic T, Imbeaud S, Imielinski M, Jäger N, Jones DT, Jones D, Knappskog S, Kool M, Lakhani SR, López-Otín C, Martin S, Munshi NC, Nakamura H, Northcott PA, Pajic M, Papaemmanuil E, Paradiso A, Pearson JV, Puente XS, Raine K, Ramakrishna M, Richardson AL, Richter J, Rosenstiel P, Schlesner M, Schumacher TN, Span PN, Teague JW, Totoki Y, Tutt AN, Valdés-Mas R, van Buuren MM, van 't Veer L, Vincent-Salomon A, Waddell N, Yates LR, Zucman-Rossi J, Futreal PA, McDermott U, Lichter P, Meyerson M, Grimmond SM, Siebert R, Campo E, Shibata T, Pfister SM, Campbell PJ, Stratton MR. Signatures of mutational processes in human cancer. *Nature*. 2013;500(7463):415-421.
30. Castro-Vega LJ, Letouzé E, Burnichon N, Buffet A, Disderot PH, Khalifa E, Loriot C, Elarouci N, Morin A, Menara M, Lepoutre-Lussey C, Badoual C, Sibony M, Dousset B, Libé R, Zinzindohoue F, Plouin PF, Bertherat J, Amar L, de Reyniès A, Favier J, Gimenez-Roqueplo AP. Multi-omics analysis defines core genomic alterations in pheochromocytomas and paragangliomas. *Nat Commun*. 2015;6:6044.
31. Flynn A, Benn D, Clifton-Bligh R, Robinson B, Trainer AH, James P, Hogg A, Waldeck K, George J, Li J, Fox SB, Gill AJ, McArthur G, Hicks RJ, Tothill RW. The genomic landscape of phaeochromocytoma. *J Pathol*. 2015;236(1):78-89.
32. Toledo RA, Qin Y, Srikantan S, Morales NP, Li Q, Deng Y, Kim SW, Pereira MA, Toledo SP, Su X, Aguiar RC, Dahia PL. In vivo and in vitro oncogenic effects of HIF2A mutations in pheochromocytomas and paragangliomas. *Endocr Relat Cancer*. 2013;20(3):349-359.
33. Rosenblum JS, Wang H, Dmitriev PM, Cappadona AJ, Mastorakos P, Xu C, Jha A, Edwards N, Donahue DR, Munasinghe J, Nazari MA, Knutsen RH, Rosenblum BR, Smirniotopoulos JG, Pappo A, Spetzler RF, Vortmeyer A, Gilbert MR, McGavern DB, Chew E, Kozel BA, Heiss JD, Zhuang Z, Pacak K. Developmental vascular malformations in EPAS1 gain-of-function syndrome. *JCI Insight*. 2021;6(5).
34. Pamporaki C, Hamplova B, Peitzsch M, Prejbisz A, Beuschlein F, Timmers H, Fassnacht M, Klink B, Lodish M, Stratakis CA, Huebner A, Fliedner S, Robledo M, Sinnott RO, Januszewicz A, Pacak K, Eisenhofer G. Characteristics of Pediatric vs Adult

Pheochromocytomas and Paragangliomas. *J Clin Endocrinol Metab*. 2017;102(4):1122-1132.

35. Eisenhofer G, Timmers HJ, Lenders JW, Bornstein SR, Tiebel O, Mannelli M, King KS, Vocke CD, Linehan WM, Bratslavsky G, Pacak K. Age at diagnosis of pheochromocytoma differs according to catecholamine phenotype and tumor location. *J Clin Endocrinol Metab*. 2011;96(2):375-384.
36. Ng SWK, Rouhani FJ, Brunner SF, Brzozowska N, Aitken SJ, Yang M, Abascal F, Moore L, Nikitopoulou E, Chappell L, Leongamornlert D, Ivovic A, Robinson P, Butler T, Sanders MA, Williams N, Coorens THH, Teague J, Raine K, Butler AP, Hooks Y, Wilson B, Birtchnell N, Naylor H, Davies SE, Stratton MR, Martincorena I, Rahbari R, Frezza C, Hoare M, Campbell PJ. Convergent somatic mutations in metabolism genes in chronic liver disease. *Nature*. 2021;598(7881):473-478.
37. Jamal-Hanjani M, Wilson GA, McGranahan N, Birkbak NJ, Watkins TBK, Veeriah S, Shafi S, Johnson DH, Mitter R, Rosenthal R, Salm M, Horswell S, Escudero M, Matthews N, Rowan A, Chambers T, Moore DA, Turajlic S, Xu H, Lee SM, Forster MD, Ahmad T, Hiley CT, Abbosh C, Falzon M, Borg E, Marafioti T, Lawrence D, Hayward M, Kolvekar S, Panagiotopoulos N, Janes SM, Thakrar R, Ahmed A, Blackhall F, Summers Y, Shah R, Joseph L, Quinn AM, Crosbie PA, Naidu B, Middleton G, Langman G, Trotter S, Nicolson M, Remmen H, Kerr K, Chetty M, Gomersall L, Fennell DA, Nakas A, Rathinam S, Anand G, Khan S, Russell P, Ezhil V, Ismail B, Irvin-Sellers M, Prakash V, Lester JF, Kornaszewska M, Attanoos R, Adams H, Davies H, Dentro S, Taniere P, O'Sullivan B, Lowe HL, Hartley JA, Iles N, Bell H, Ngai Y, Shaw JA, Herrero J, Szallasi Z, Schwarz RF, Stewart A, Quezada SA, Le Quesne J, Van Loo P, Dive C, Hackshaw A, Swanton C. Tracking the Evolution of Non-Small-Cell Lung Cancer. *N Engl J Med*. 2017;376(22):2109-2121.
38. Shimizu S, Eguchi Y, Kamiike W, Itoh Y, Hasegawa J, Yamabe K, Otsuki Y, Matsuda H, Tsujimoto Y. Induction of apoptosis as well as necrosis by hypoxia and predominant prevention of apoptosis by Bcl-2 and Bcl-XL. *Cancer Res*. 1996;56(9):2161-2166.
39. Lee S, Nakamura E, Yang H, Wei W, Linggi MS, Sajan MP, Farese RV, Freeman RS, Carter BD, Kaelin WG, Jr., Schlisio S. Neuronal apoptosis linked to EglN3 prolyl hydroxylase and familial pheochromocytoma genes: developmental culling and cancer. *Cancer Cell*. 2005;8(2):155-167.
40. Ko CY, Tsai MY, Tseng WF, Cheng CH, Huang CR, Wu JS, Chung HY, Hsieh CS, Sun CK, Hwang SP, Yuh CH, Huang CJ, Pai TW, Tzou WS, Hu CH. Integration of CNS survival and differentiation by HIF2α. *Cell Death Differ*. 2011;18(11):1757-1770.
41. Bechmann N, Moskopp ML, Ullrich M, Calsina B, Wallace PW, Richter S, Friedemann M, Langton K, Fliedner SMJ, Timmers H, Nölting S, Beuschlein F, Fassnacht M, Prejbisz A,

Pacak K, Ghayee HK, Bornstein SR, Dieterich P, Pietzsch J, Wielockx B, Robledo M, Qin N, Eisenhofer G. HIF2α supports pro-metastatic behavior in pheochromocytomas/paragangliomas. *Endocr Relat Cancer*. 2020;27(11):625-640.

42. Bechmann N, Eisenhofer G. Hypoxia-inducible Factor 2α: A Key Player in Tumorigenesis and Metastasis of Pheochromocytoma and Paraganglioma? *Exp Clin Endocrinol Diabetes*. 2021.
43. Ben Aim L, Pigny P, Castro-Vega LJ, Buffet A, Amar L, Bertherat J, Drui D, Guilhem I, Baudin E, Lussey-Lepoutre C, Corsini C, Chabrier G, Briet C, Faivre L, Cardot-Bauters C, Favier J, Gimenez-Roqueplo AP, Burnichon N. Targeted next-generation sequencing detects rare genetic events in pheochromocytoma and paraganglioma. *J Med Genet*. 2019;56(8):513-520.
44. Bhandari V, Hoey C, Liu LY, Lalonde E, Ray J, Livingstone J, Lesurf R, Shiah YJ, Vujcic T, Huang X, Espiritu SMG, Heisler LE, Yousif F, Huang V, Yamaguchi TN, Yao CQ, Sabelnykova VY, Fraser M, Chua MLK, van der Kwast T, Liu SK, Boutros PC, Bristow RG. Molecular landmarks of tumor hypoxia across cancer types. *Nat Genet*. 2019;51(2):308-318.
45. Tang M, Bolderson E, O'Byrne KJ, Richard DJ. Tumor Hypoxia Drives Genomic Instability. *Front Cell Dev Biol*. 2021;9:626229.
46. Bristow RG, Hill RP. Hypoxia and metabolism. Hypoxia, DNA repair and genetic instability. *Nat Rev Cancer*. 2008;8(3):180-192.
47. Comino-Méndez I, de Cubas AA, Bernal C, Álvarez-Escolá C, Sánchez-Malo C, Ramírez-Tortosa CL, Pedrinaci S, Rapizzi E, Ercolino T, Bernini G, Bacca A, Letón R, Pita G, Alonso MR, Leandro-García LJ, Gómez-Graña A, Inglada-Pérez L, Mancikova V, Rodríguez-Antona C, Mannelli M, Robledo M, Cascón A. Tumoral EPAS1 (HIF2A) mutations explain sporadic pheochromocytoma and paraganglioma in the absence of erythrocytosis. *Hum Mol Genet*. 2013;22(11):2169-2176.
48. Oster ME, Lee KA, Honein MA, Riehle-Colarusso T, Shin M, Correa A. Temporal trends in survival among infants with critical congenital heart defects. *Pediatrics*. 2013;131(5):e1502-1508.
49. Ponz de Antonio I, Ruiz Cantador J, González García AE, Oliver Ruiz JM, Sánchez-Recalde Á, López-Sendón JL. Prevalence of Neuroendocrine Tumors in Patients With Cyanotic Congenital Heart Disease. *Rev Esp Cardiol (Engl Ed)*. 2017;70(8):673-675.

Figure legends:

Figure 1. Results of whole exome sequencing in CCHD-PPGL

a, Landscape of genetic alterations in 16 CCHD-PPGL samples from seven patients. Number of silent and non-silent somatic mutations is displayed above. Case number, age at operation/autopsy, tumor type and sample type, together with the types of mutations and copy number alterations are shown by color as indicated. Frequency of affected samples is shown on the right. PGL, paraganglioma; PCC, pheochromocytoma; AMH, adrenal medullary hyperplasia; FFPE, formalin-fixed paraffin-embedded tissue; FF, fresh frozen tissue. **b,** Mutation spectrum in CCHD-PPGL. **c,** Distribution of *EPAS1* mutations in CCHD-PPGL samples.

Figure 2. Comparison of genetic profiles between CCHD-PPGL and non-CCHD-PPGL

a, Landscape of genetic alterations in 173 non-CCHD-PPGL (TCGA-PPGL) samples. Genes associated with hypoxia signaling are shown in red. Types of mutations and copy number alterations are shown by different colors as indicated. Frequency of affected samples is shown on the right. CN-LOH, copy neutral loss of heterozygosity. **b,** Comparisons of frequency of common copy number alterations between CCHD-PPGL (n = 16, red) and non-CCHD-PPGL (n = 173, bule) or non-CCHD-PPGL with mutations in hypoxia related genes (n = 37, turquoise-blue). Significant difference in frequency is shown by asterisks ($q < 0.1$, two-sided Fisher's exact test with Benjamini-Hochberg adjustment for multiple testing). **c-d,** Forest plots showing enrichment of *EPAS1* mutation and copy number alterations between CCHD-PPGL and non-CCHD-PPGL (c) or non-CCHD-PPGL with mutations in hypoxia related genes (d) with 95% confidence interval. Significant enrichment in CCHD-PPGL is shown in red, while significant enrichment in non-CCHD-PPGL or non-CCHD-PPGL with mutations in hypoxia related genes is displayed in blue or turquoise-blue (two-sided Fisher's exact test). *EPAS1* mut, *EPAS1* mutation; del, deletion; amp, amplification; OR, odds ratio.

Figure 3. Parallel evolution of multiple *EPAS1*-mutated tumors in CCHD patients

a-c, Tumor location (left) and variant allele frequency for somatic mutations (right) of multifocal CCHD-PPGLs from Case 1-3. Three and six tumors (indicated by "TX") were resected from Case 1 and 2, whereas two tumors and an AMH sample were obtained from Case 3. Age at operation is shown above. Variant allele frequency is plotted for all somatic mutations in each PPGL/AMH. No shared mutations were detected in multifocal PPGL/AMH samples from these three cases. Unique *EPAS1* mutations (red) are indicated by arrowheads. **d**, Copy number profiles of all PPGL/AMH samples from Case 1-3. Each line represents the profile of a tumor, with amplification in red and deletion in blue. Del, deletion; Amp, amplification. **e**, A hypothetical model of CCHD-PPGL development and the role of hypoxemia, *EPAS1* mutations and additional genetic hits.

Hypoxemia imposes a strong selective pressure that favors *EPAS1*-mutated cells. However, it could no longer be required for further selection of *EPAS1*-mutated clones that acquire additional genetic hits, such as 11p deletions and 2p amplifications, for CCHD-PPGL development.

Table 1. Clinical features of seven patients with CCHD-PPGL

Patient No.	Sex	Form of cyanotic congenital heart disease	Duration of cyanosis (y)	SaO2 at PPGL diagnosis (%)	Hematocrit at PPGL diagnosis (%)	Age at initial PPGL diagnosis (yr)	PPGL location and Size	Sample type	Somatic *EPAS1* mutations
1	F	Atrioventricular septal defect, Double outlet left ventricle, Pulmonary stenosis, Total anomalous pulmonary venous return, Absence of the inferior vena cava, Azygos connection, Right aortic arch	26	77	53.6	26	(1)Retroperitoneal PGL : 4.2 x 2.8cm (2)Left adrenal PCC : 1.8 x 1.3cm (3)Retroperitoneal PGL : 2.0 x 2.0cm	FF	(1)c.1591C>T, p.Pro531Ser (2)c.1625T>G, p.Leu542Arg (3)c.1594T>A, p.Tyr532Asn
2	M	Double outlet right ventricle, Pulmonary atresia	12	95	43.7	19	(1)Retroperitoneal PGL : 1.7 x 1.2cm (2)Retroperitoneal PGL : 1.7 x 1.0cm (3)Retroperitoneal PGL : 0.6 x 0.5cm (4)Retroperitoneal PGL : 1.8 x 2.0cm (5)Retroperitoneal PGL : 2.1 x 1.2cm (6)Retroperitoneal PGL : 0.8 x 0.7cm	(1)-(3) FFPE (4)-(6) FF	(1)c.1591C>A, p.Pro531Thr (2)c.1616A>C, p.Asp539Ala (3)c.1589C>T, p.Ala530Val (4)c.1591C>T, p.Pro531Ser (5)c.1598T>A, p.Ile533Asn (6)c.1588G>C, p.Ala530Pro
3	F	Double outlet right ventricle, Eisenmenger syndrome	32	50	61.3	32	(1)Left adrenal PCC : 11.0 x 7.0cm (2)Right AMH (3)Urinary bladder PGL : 0.4 x 0.2cm	FFPE	(1)c.1599C>G, p.Ile533Met (2)c.1592C>T, p.Pro531Leu (3)WT
4	M	Double outlet right ventricle, Pulmonary atresia	46	82	39.8	46	Left adrenal PCC : 1.0 x 1.0cm	FFPE	c.1591C>T, p.Pro531Ser
5	F	Single ventricle, Pulmonary atresia	20	78	40.5	20	Retroperitoneal PGL : 3.0 x 2.7cm	FFPE	c.1591C>T, p.Pro531Ser
6	M	Hypoplastic left heart syndrome, Aortic valve atresia, Mitral atresia	18	90	53.0	18	Retroperitoneal PGL : 1.8 x 1.6cm	FFPE	c.1589C>G, p.Ala530Gly

7	F	Double outlet right ventricle, Pulmonary atresia, Total anomalous pulmonary venous connection, Atrioventricular septal defect	33	80	41.1	33	Retroperitoneal PGL : 3.1 x 2.5cm	FFPE	c.1595A>G, p.Tyr532Cys

SaO2, arterial oxygen saturation; PCC, pheochromocytoma; PGL, extra-adrenal paraganglioma; FF, fresh frozen tissue; FFPE, formalin-fixed paraffin-embedded tissue.

Table 2. Clinical characteristics of patients with CCHD-PPGL as compared with non-CCHD-PPGL from the TCGA cohort

Clinical characteristics	CCHD (n=7)	Non-CCHD-PPGL with mutations in hypoxia related genes (n=29)	Non-CCHD-PPGL without mutations in hypoxia related genes (n=136)
Median age at initial diagnosis of PPGLs -yr (range)	26 (18-46)	39 (19-72)†	46 (20-83)†
Female -no. (%)	4 (57)	14 (48)	78 (57)
Occurrence of PGL -no. (%)	6 (86)	18 (62)	10 (7)‡
Bilateral adrenal PCC -no. (%)	0 (0)	2 (7)	8 (6)
Multifocal PPGLs (excluding only bilateral PCC) -no. (%)	3 (43)	7 (24)	3 (2)‡
Metastatic disease -no. (%)	1 (14)	4 (14)	7 (5)

PGL, extra-adrenal paraganglioma; PCC, pheochromocytoma.

† Denotes an older age ($p < 0.05$) than patients with CCHD-PPGL.

‡ Denotes a lower frequency ($p < 0.05$) than patients with CCHD-PPGL.

Figure1

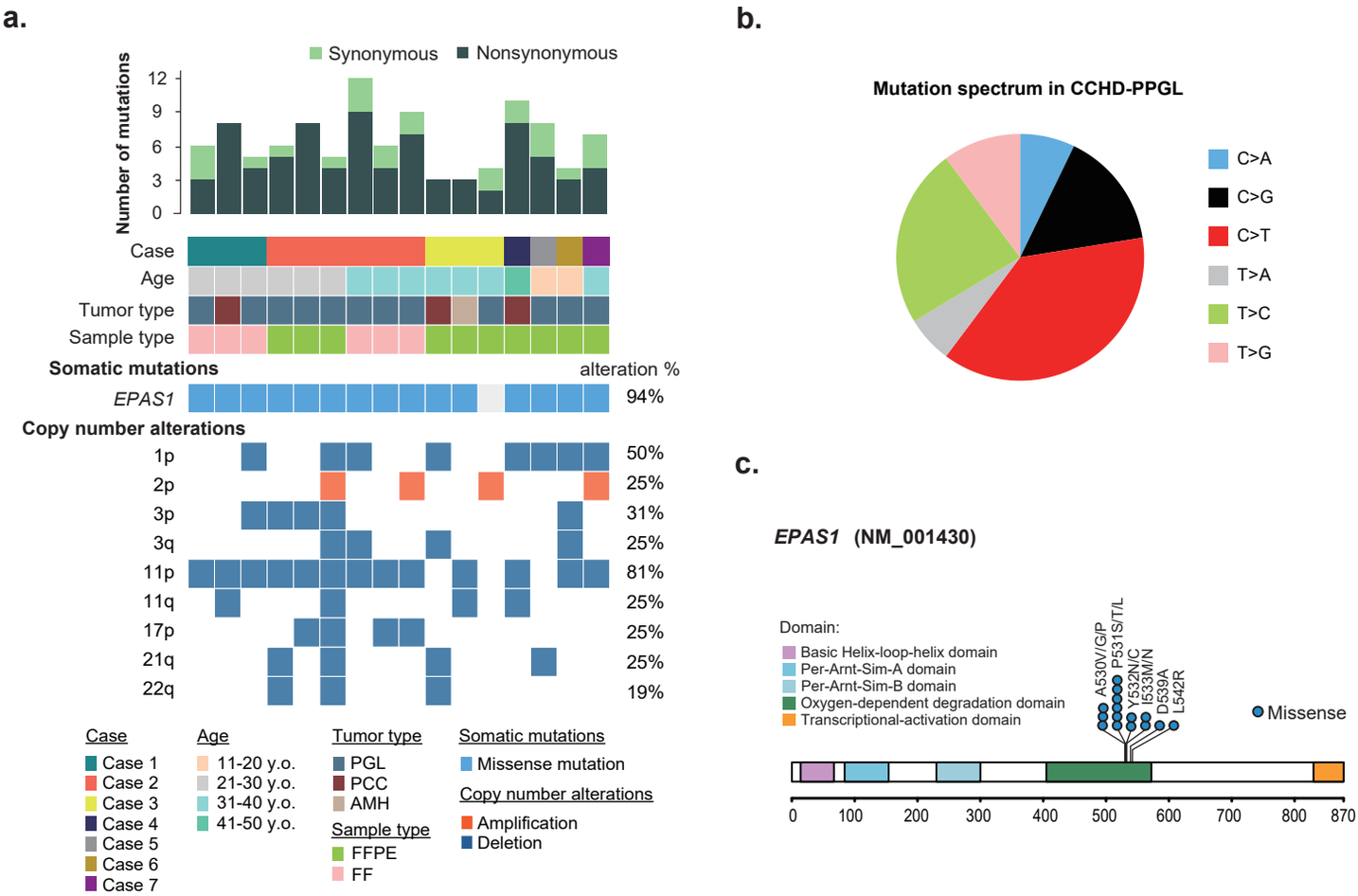
a.
Synonymous
Nonsynonymous
Number of mutations
12
9
6
3
0
Case
Age
Tumor type
Sample type
Somatic mutations
alteration %
EPAS1
94%
Copy number alterations
1p
2p
3p
3q
11p
11q
17p
21q
22q
50%
25%
31%
25%
81%
25%
25%
25%
19%
Case
Case 1
Case 2
Case 3
Case 4
Case 5
Case 6
Case 7
Age
11-20 y.o.
21-30 y.o.
31-40 y.o.
41-50 y.o.
Tumor type
PGL
PCC
AMH
Sample type
FFPE
FF
Somatic mutations
Missense mutation
Copy number alterations
Amplification
Deletion
b.
Mutation spectrum in CCHD-PPGL
C>A
C>G
C>T
T>A
T>C
T>G
c.
EPAS1 (NM_001430)
Domain:
Basic Helix-loop-helix domain
Per-Arnt-Sim-A domain
Per-Arnt-Sim-B domain
Oxygen-dependent degradation domain
Transcriptional-activation domain
A530V/G/P
P531S/T/L
Y532N/C
I533M/N
D539A
L542R
Missense
0
100
200
300
400
500
600
700
800
870

Figure2

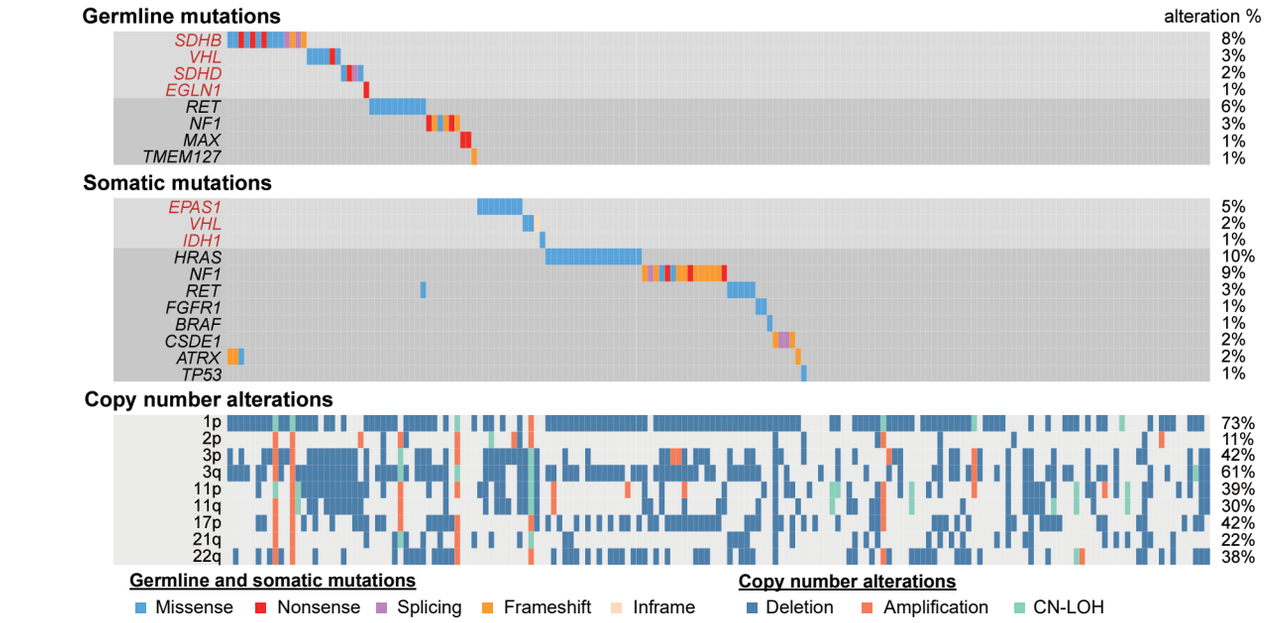
a.
Germline mutations
alteration %
SDHB 8%
VHL 3%
SDHD 2%
EGLN1 1%
RET 6%
NF1 3%
MAX 1%
TMEM127 1%
Somatic mutations
EPAS1 5%
VHL 2%
IDH1 1%
HRAS 10%
NF1 9%
RET 3%
FGFR1 1%
BRAF 1%
CSDE1 2%
ATRX 2%
TP53 1%
Copy number alterations
1p 73%
2p 11%
3p 42%
3q 61%
11p 39%
11q 30%
17p 42%
21q 22%
22q 38%
Germline and somatic mutations
Missense
Nonsense
Splicing
Frameshift
Inframe
Copy number alterations
Deletion
Amplification
CN-LOH

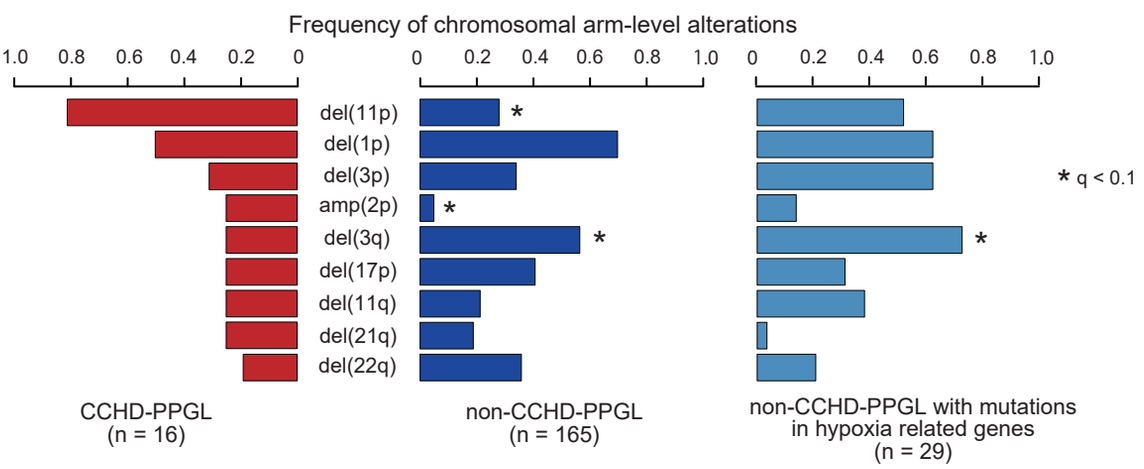
b.
Frequency of chromosomal arm-level alterations
1.0 0.8 0.6 0.4 0.2 0
0 0.2 0.4 0.6 0.8 1.0
0 0.2 0.4 0.6 0.8 1.0
del(11p)
del(1p)
del(3p)
amp(2p)
del(3q)
del(17p)
del(11q)
del(21q)
del(22q)
* q < 0.1
CCHD-PPGL
(n = 16)
non-CCHD-PPGL
(n = 165)
non-CCHD-PPGL with mutations
in hypoxia related genes
(n = 29)

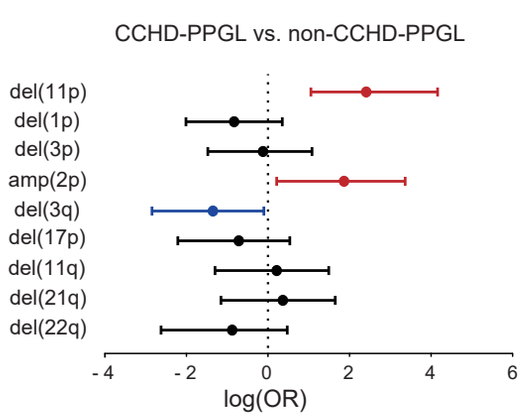
c.
CCHD-PPGL vs. non-CCHD-PPGL
del(11p)
del(1p)
del(3p)
amp(2p)
del(3q)
del(17p)
del(11q)
del(21q)
del(22q)
- 4 - 2 0 2 4 6
log(OR)

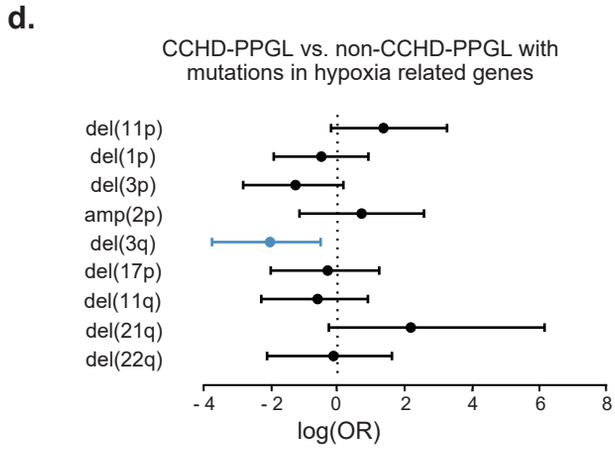
d.
CCHD-PPGL vs. non-CCHD-PPGL with
mutations in hypoxia related genes
del(11p)
del(1p)
del(3p)
amp(2p)
del(3q)
del(17p)
del(11q)
del(21q)
del(22q)
- 4 - 2 0 2 4 6 8
log(OR)

Figure3

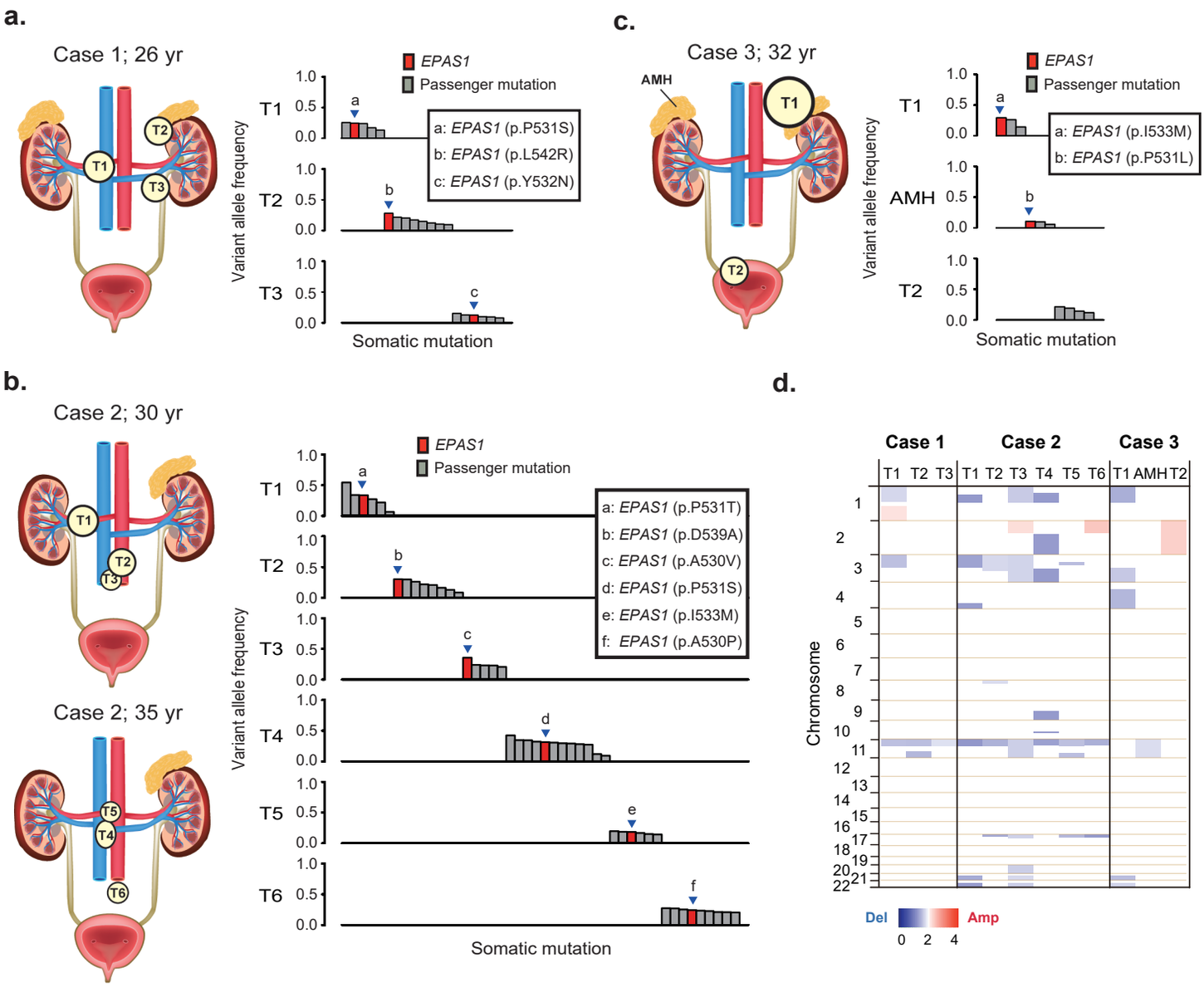
a.
Case 1; 26 yr
T1
T2
T3
EPAS1
Passenger mutation
a: EPAS1 (p.P531S)
b: EPAS1 (p.L542R)
c: EPAS1 (p.Y532N)
Variant allele frequency
Somatic mutation
c.
Case 3; 32 yr
AMH
a: EPAS1 (p.I533M)
b: EPAS1 (p.P531L)
b.
Case 2; 30 yr
Case 2; 35 yr
T4
T5
T6
a: EPAS1 (p.P531T)
b: EPAS1 (p.D539A)
c: EPAS1 (p.A530V)
d: EPAS1 (p.P531S)
e: EPAS1 (p.I533M)
f: EPAS1 (p.A530P)
d.
Case 1
Case 2
Case 3
Chromosome
Del
Amp

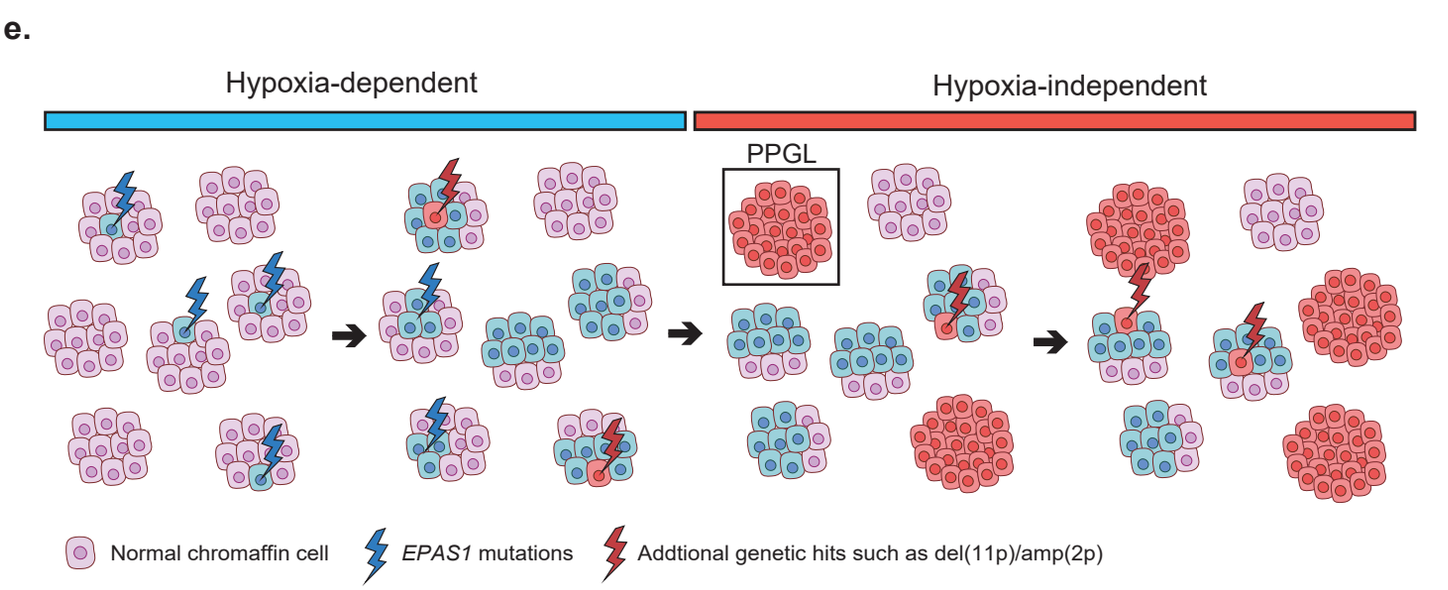
e.
Hypoxia-dependent
Hypoxia-independent
PPGL
Normal chromaffin cell
EPAS1 mutations
Addtional genetic hits such as del(11p)/amp(2p)

Supplementary Figure 1

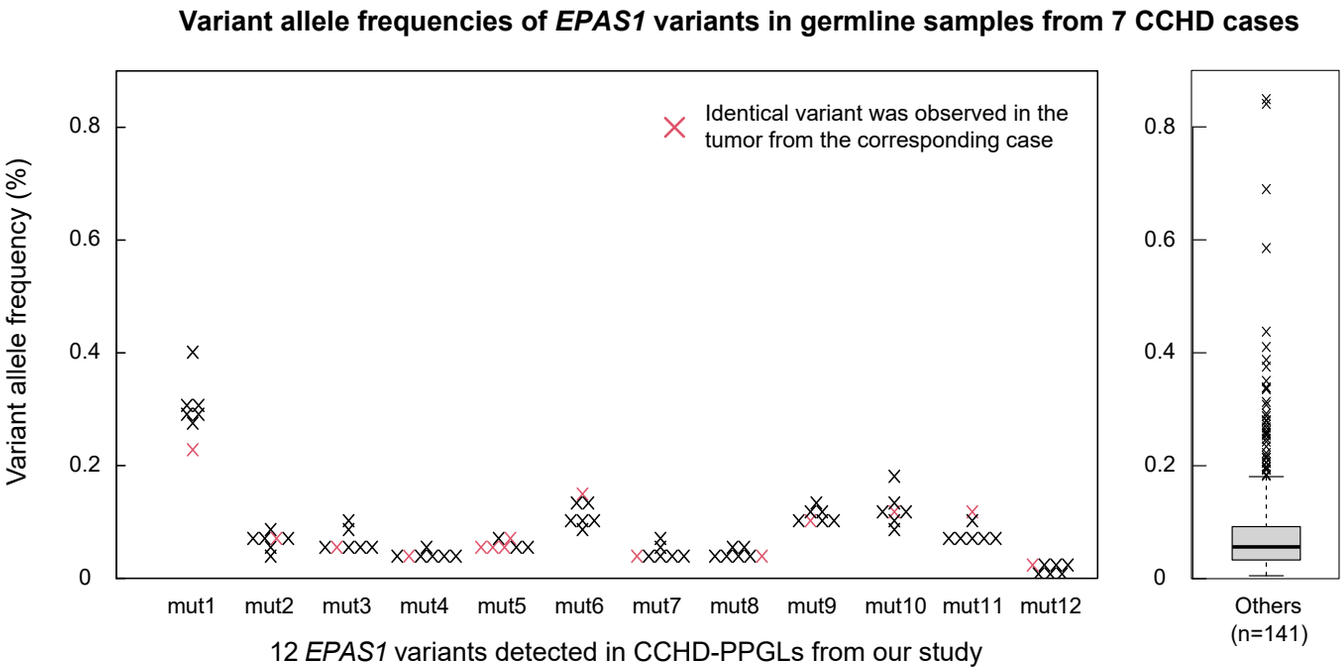

* Variant allele frequency (VAF) in seven germline samples is plotted for all 12 *EPAS1* variants detected in CCHD-PPGLs. Red point represents the VAF of identical variants which was observed in the tumor from the corresponding case. VAFs of artifact variants in all germline samples were also shown on the right side of the figure.

Supplementary Figure 2

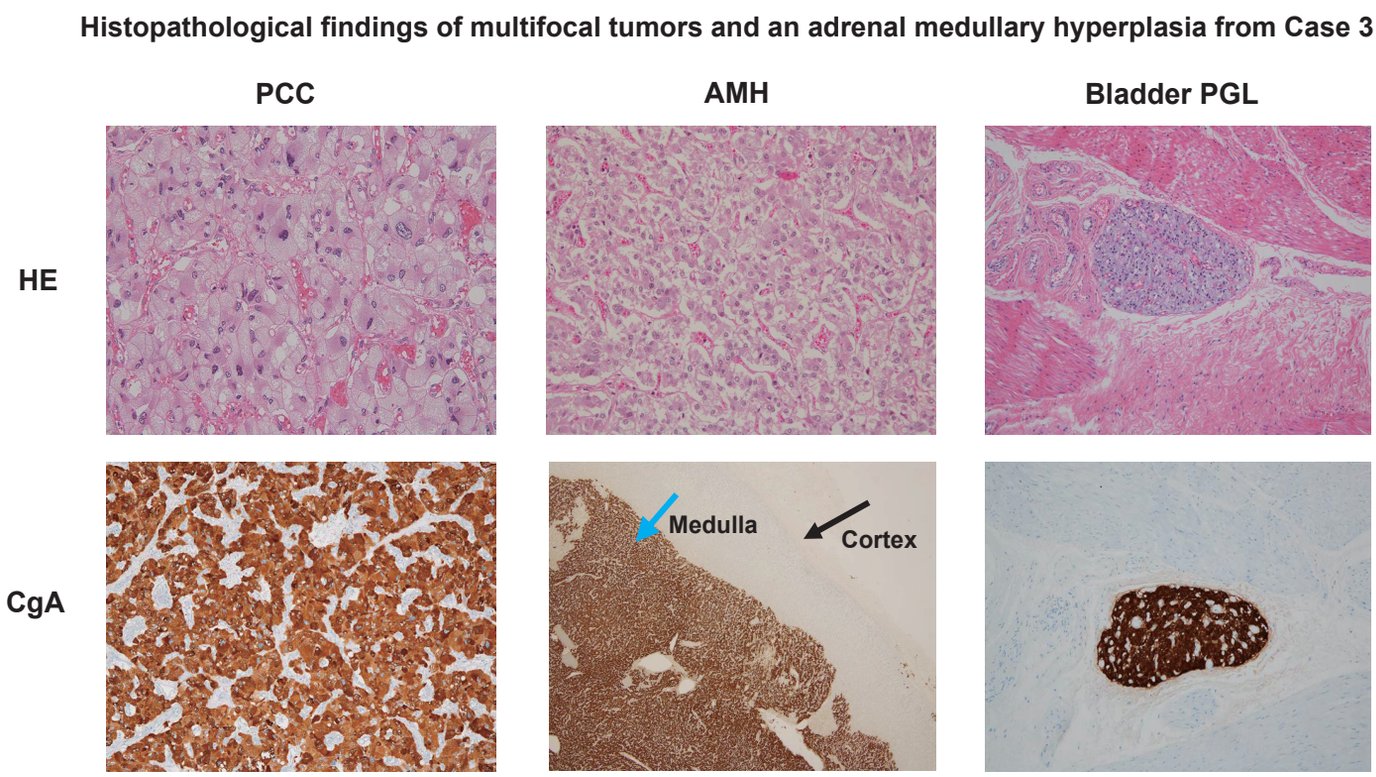

* Hematoxylin and eosin (HE) staining and immunohistochemistry for chromogranin A (CgA) of a pheochromocytoma (PCC), an adrenal medullary hyperplasia (AMH) and a microscopic bladder paraganglioma (PGL) from Case 3. AMH represents a substantial widening of the adrenal medulla, indicated by a blue arrowhead. Tumor and AMH cells showed positive chromogranin A staining.

Supplementary Table 1. Clinical and biochemical features of seven patients presenting with cyanotic congenital heart disease (CCHD) and pheochromocytomas or paragangliomas (PPGLs).

Patient No.	Sex	Description of Cyanotic Congenital Heart Disease and Treatment	Duration of Cyanosis (y)	SaO2 at PPGL diagnosis (%)	HCT (%) Hgb (g/dl) at PPGL diagnosis	Somatostatinoma	Clinical presentation leading to PPGL diagnosis	Age at initial PPGL diagnosis (yr)	Catecholamines	PPGL/AMH location and size	Sample type	Somatic *EPAS1* mutations
1	F	Atrioventricular septal defect, Double-outlet left ventricle, Pulmonary stenosis, Total anomalous pulmonary venous return, Absence of the inferior vena cava, Azygos connection, Right aortic arch Treatment: No cardiac procedures	26	77	53.6/15.1	No	Abdominal pain, vomiting, tachycardia, diaphroesis	26	U-NMN, 9×; U-MN, normal	(1)Retroperitoneal PGL : 4.2 x 2.8cm (2)Left adrenal PCC : 1.8 x 1.3cm (3)Retroperitoneal PGL : 2.0 x 2.0cm	(1)-(3) FF	(1)c.1591C>T, p.Pro531Ser (2)c.1625T>G, p.Leu542Arg (3)c.1594T>A, p.Tyr532Asn
2	M	Double outlet right ventricle, Pulmonary atresia Treatment: Left BTS at 3 yr; Right BTS at 5 yr; Glenn shunt at 7 yr; Fontan procedure at 12 yr	12	95	43.7/13.8	No	Hypertension, dyspnea, diaphroesis	19	U-NMN, 7×; U-MN, normal	(1)Retroperitoneal PGL : 1.7 x 1.2cm (2)Retroperitoneal PGL : 1.7 x 1.0cm (3)Retroperitoneal PGL : 0.6 x 0.5cm (4)Retroperitoneal PGL : 1.8 x 2.0cm (5)Retroperitoneal PGL : 2.1 x 1.2cm (6)Retroperitoneal PGL : 0.8 x 0.7cm	(1)-(3) FFPE (4)-(6) FF	(1)c.1591C>A, p.Pro531Thr (2)c.1616A>C, p.Asp539Ala (3)c.1589C>T, p.Ala530Val (4)c.1591C>T, p.Pro531Ser (5)c.1598T>A, p.Ile533Asn (6)c.1588G>C, p.Ala530Pro
3	F	Double outlet right ventricle, Eisenmenger syndrome Treatment: No cardiac procedures	32	50	61.3/17.5	No	Abdominal pain, tachycardia, hypertension	32	U-NMN, 65×; U-MN, 18×	(1)Left adrenal PCC : 11.0 x 7.0cm (2)Right AMH (3)Urinary bladder PGL : 0.4 x 0.2cm	(1)-(3) FFPE	(1)c.1599C>G, p.Ile533Met (2)c.1592C>T, p.Pro531Leu (3)WT
4	M	Double outlet right ventricle, Pulmonary atresia Treatment: Left BTS at 4 yr; Right BTS at 14 and 36 yr	46	82	39.8/12.6	No	None	46	U-NMN, <2×; U-MN, normal	Left adrenal PCC : 1.0 x 1.0cm	FFPE	c.1591C>T, p.Pro531Ser
5	F	Single ventricle, Pulmonary atresia Treatment: Left BTS at 1 month of age; Right BTS at 3 yr; Glenn shunt at 6 yr; Fontan procedure at 11 yr (failure)	20	78	40.5/14.0	No	Hypertension, tachcardia, nausea,abdominal pain	20	U-NAD, 38×; U-AD, normal	Retroperitoneal PGL : 3.0 x 2.7cm	FFPE	c.1591C>T, p.Pro531Ser
6	M	Hypoplastic left heart syndrome, Aortic valve atresia, Mitral atresia Treatment: Norwood procedure at 14 days of age; Glenn shunt at 6 months of age; Fontan procedure at 2 yr (failure)	18	75	53.0/17.9	No	Hypertension, tachycardia, dyspnea, diaphroesis, headache	18	U-NAD, 10×; U-AD, normal	Retroperitoneal PGL : 1.8 x 1.6cm	FFPE	c.1589C>G, p.Ala530Gly
7	F	Double outlet right ventricle, Pulmonary atresia, Total anomalous pulmonary venous connection, Atrioventricular septal defect Treatment: Right BTS 1 yr; Glenn shunt at 19 yr	33	80	41.1/12.3	No	Headache, palpitations	33	U-NMN, 4×; U-MN, normal	Retroperitoneal PGL : 3.1 x 2.5cm	FFPE	c.1595A>G, p.Tyr532Cys

BTS, Blalock-Taussig shunt; U-NMN, urinary normetanephrine; U-MN, urinary metanephrine; U-NAD, urinary noradrenaline; U-AD, urinary adrenaline; PGL, paraganglioma; PCC, pheochromocytoma; FF, fresh frozen tissue; FFPE, formalin-fixed paraffin-embedded tissue

Supplementary Table 2. Summary of somatic mutations of CCHD-PPGLs detected by whole exome sequencing.

Sample ID	Chr *	Start	End	Ref	Alt	Gene	Type of mutations	VAF
C1-T1	1	117492019	117492019	T	G	*PTGFRN*	synonymous SNV	0.256
C1-T1	20	3766778	3766778	G	A	*CENPB*	nonsynonymous SNV	0.239437
C1-T1	2	46607402	46607402	C	T	*EPAS1*	nonsynonymous SNV	0.246575
C1-T1	8	146017163	146017163	T	G	*RPL8*	nonsynonymous SNV	0.171875
C1-T1	10	27326820	27326820	C	A	*ANKRD26*	nonsynonymous SNV	0.13253
C1-T2	2	46607436	46607436	T	G	*EPAS1*	nonsynonymous SNV	0.28169
C1-T2	2	55522809	55522809	C	A	*CCDC88A*	nonsynonymous SNV	0.20339
C1-T2	16	1270496	1270496	C	-	*CACNA1H*	frameshift deletion	0.216667
C1-T2	X	7811584	7811584	C	T	*VCX*	nonsynonymous SNV	0.172414
C1-T2	6	28963716	28963716	C	T	*ZNF311*	nonsynonymous SNV	0.148515
C1-T2	6	157528133	157528133	G	A	*ARID1B*	nonsynonymous SNV	0.123188
C1-T2	17	41582151	41582151	G	T	*DHX8*	nonsynonymous SNV	0.104651
C1-T2	17	48217519	48217519	T	A	*PPP1R9B*	nonsynonymous SNV	0.095652
C1-T3	11	58861957	58861957	G	A	*GLYATL1B*	nonsynonymous SNV	0.152542
C1-T3	2	46607405	46607405	T	A	*EPAS1*	nonsynonymous SNV	0.125
C1-T3	10	90524196	90524196	G	T	*LIPN*	nonsynonymous SNV	0.127907
C1-T3	7	142997033	142997033	G	A	*CASP2*	synonymous SNV	0.099237
C1-T3	11	102248273	102248273	A	G	*BIRC2*	synonymous SNV	0.094828
C1-T3	2	26540377	26540377	C	T	*ADGRF3*	synonymous SNV	0.079365
C2-T1	4	154625859	154625859	G	A	*TLR2*	synonymous SNV	0.545455
C2-T1	17	46703586	46703586	T	C	*HOXB9*	nonsynonymous SNV	0.340659
C2-T1	2	46607402	46607402	C	A	*EPAS1*	nonsynonymous SNV	0.337079
C2-T1	19	17013510	17013510	G	A	*CPAMD8*	nonsynonymous SNV	0.272727
C2-T1	16	27221704	27221704	T	C	*KDM8*	nonsynonymous SNV	0.219512
C2-T1	5	90008116	90008116	G	A	*ADGRV1*	nonsynonymous SNV	0.065574
C2-T2	16	5038148	5038148	A	C	*SEC14L5*	splicing	0.261682
C2-T2	2	46607427	46607427	A	C	*EPAS1*	nonsynonymous SNV	0.302083
C2-T2	19	1008723	1008723	T	C	*GRIN3B*	nonsynonymous SNV	0.298077
C2-T2	X	104999225	104999225	T	C	*IL1RAPL2*	nonsynonymous SNV	0.207792
C2-T2	6	34059876	34059876	T	G	*GRM4*	nonsynonymous SNV	0.162162
C2-T2	3	196792217	196792217	A	G	*DLG1*	nonsynonymous SNV	0.218487
C2-T2	8	145641195	145641195	G	A	*SLC39A4*	nonsynonymous SNV	0.129032
C2-T2	8	16021685	16021685	A	T	*MSR1*	nonsynonymous SNV	0.085106
C2-T3	2	46607400	46607400	C	T	*EPAS1*	nonsynonymous SNV	0.356436
C2-T3	4	106157657	106157657	T	G	*TET2*	nonsynonymous SNV	0.229358
C2-T3	2	29295925	29295925	T	G	*PCARE*	synonymous SNV	0.230769
C2-T3	16	70713757	70713757	T	C	*MTSS2*	nonsynonymous SNV	0.206897
C2-T3	1	155730368	155730368	A	G	*GON4L*	nonsynonymous SNV	0.239437
C2-T4	8	119593081	119593081	T	C	*SAMD12*	nonsynonymous SNV	0.424242
C2-T4	2	15427184	15427198	ACTGTGT	-	*NBAS*	frameshift deletion	0.346667
C2-T4	20	60768647	60768647	C	-	*MTG2*	frameshift deletion	0.344538
C2-T4	17	62018426	62018426	C	T	*SCN4A*	nonsynonymous SNV	0.321739
C2-T4	2	46607402	46607402	C	T	*EPAS1*	nonsynonymous SNV	0.31401
C2-T4	19	45856063	45856063	C	T	*ERCC2*	nonsynonymous SNV	0.306452
C2-T4	11	63487651	63487651	C	G	*RTN3*	synonymous SNV	0.295775
C2-T4	1	248366742	248366742	G	C	*OR2M3*	nonsynonymous SNV	0.291429
C2-T4	11	66610688	66610688	C	G	*C11orf80*	nonsynonymous SNV	0.280899
C2-T4	1	6169862	6169862	C	T	*CHD5*	synonymous SNV	0.272727
C2-T4	3	49449876	49449905	CTGGGCA	-	*TCTA*	frameshift deletion	0.12
C2-T4	2	137988741	137988741	T	C	*THSD7B*	synonymous SNV	0.093023
C2-T5	11	57995718	57995718	G	A	*OR10Q1*	synonymous SNV	0.196262

C2-T5	1	231402073	231402073	T	C	*GNPAT*	synonymous SNV	0.186047
C2-T5	2	46607409	46607409	T	A	*EPAS1*	nonsynonymous SNV	0.183432
C2-T5	1	171514665	171514665	A	G	*PRRC2C*	nonsynonymous SNV	0.166667
C2-T5	2	74761331	74761331	C	T	*LOXL3*	nonsynonymous SNV	0.150538
C2-T5	19	42794536	42794536	C	G	*CIC*	nonsynonymous SNV	0.142857
C2-T6	16	48175230	48175230	C	T	*ABCC12*	nonsynonymous SNV	0.274809
C2-T6	16	88643720	88643720	A	G	*ZC3H18*	synonymous SNV	0.270833
C2-T6	19	50752987	50752987	G	A	*MYH14*	synonymous SNV	0.253968
C2-T6	2	46607399	46607399	G	C	*EPAS1*	nonsynonymous SNV	0.243119
C2-T6	8	22995385	22995385	A	G	*TNFRSF10D*	stoploss	0.235294
C2-T6	20	5904390	5904406	AGCCATT	-	*CHGB*	frameshift deletion	0.227273
C2-T6	11	51411516	51411516	C	A	*OR4A5*	nonsynonymous SNV	0.211765
C2-T6	11	82895767	82895767	A	G	*PCF11*	nonsynonymous SNV	0.20979
C2-T6	22	19463121	19463121	G	C	*UFD1*	nonsynonymous SNV	0.204918
C3-T1	2	46607410	46607410	C	G	*EPAS1*	nonsynonymous SNV	0.292308
C3-T1	19	16982177	16982177	A	C	*SIN3B*	nonsynonymous SNV	0.261538
C3-T1	4	17805191	17805191	T	C	*DCAF16*	nonsynonymous SNV	0.142857
C3-AMH	2	46607403	46607403	C	T	*EPAS1*	nonsynonymous SNV	0.104167
C3-AMH	5	121187737	121187737	G	A	*FTMT*	nonsynonymous SNV	0.097713
C3-AMH	12	95387962	95387962	T	C	*NDUFA12*	nonsynonymous SNV	0.056818
C3-T2	10	93768011	93768011	T	A	*BTAF1*	synonymous SNV	0.213333
C3-T2	17	7721755	7721755	G	A	*DNAH2*	nonsynonymous SNV	0.191176
C3-T2	22	39884240	39884240	C	T	*MGAT3*	synonymous SNV	0.141844
C3-T2	1	11115113	11115113	G	T	*SRM*	nonsynonymous SNV	0.117188
C4-T	4	37327629	37327629	T	C	*NWD2*	nonsynonymous SNV	0.293333
C4-T	2	46607402	46607402	C	T	*EPAS1*	nonsynonymous SNV	0.269663
C4-T	19	35829217	35829217	G	A	*CD22*	nonsynonymous SNV	0.243243
C4-T	2	21230333	21230333	C	T	*APOB*	nonsynonymous SNV	0.210145
C4-T	4	126241604	126241604	C	T	*FAT4*	synonymous SNV	0.16129
C4-T	1	119964749	119964749	G	C	*HSD3B2*	nonsynonymous SNV	0.142857
C4-T	1	1139108	1139108	A	G	*TNFRSF18*	nonsynonymous SNV	0.098901
C4-T	1	33490134	33490134	T	C	*AK2*	nonsynonymous SNV	0.075758
C4-T	22	46134689	46134689	G	C	*ATXN10*	nonsynonymous SNV	0.072
C4-T	9	33258981	33258983	CTT	-	*BAG1*	nonframeshift deletion	0.084849
C5-T	12	4919754	4919754	G	A	*KCNA6*	nonsynonymous SNV	0.631579
C5-T	11	62287224	62287224	G	A	*AHNAK*	nonsynonymous SNV	0.506849
C5-T	2	46607402	46607402	C	T	*EPAS1*	nonsynonymous SNV	0.373134
C5-T	1	172013546	172013546	T	C	*DNM3*	synonymous SNV	0.31068
C5-T	9	101546397	101546397	C	G	*ANKS6*	nonsynonymous SNV	0.372093
C5-T	11	4842988	4842988	G	C	*OR51F2*	nonsynonymous SNV	0.306452
C5-T	2	201437349	201437349	C	T	*SGO2*	synonymous SNV	0.130952
C5-T	12	119968730	119968730	C	T	*CCDC60*	synonymous SNV	0.054546
C6-T	2	46607400	46607400	C	G	*EPAS1*	nonsynonymous SNV	0.29703
C6-T	12	91357935	91357935	A	T	*EPYC*	nonsynonymous SNV	0.25
C6-T	2	42867361	42867361	A	G	*MTA3*	synonymous SNV	0.180328
C6-T	7	72892157	72892157	T	G	*BAZ1B*	nonsynonymous SNV	0.084906
C7-T	3	45583346	45583346	C	G	*LARS2*	synonymous SNV	0.373333
C7-T	16	28900268	28900268	C	G	*ATP2A1*	synonymous SNV	0.311688
C7-T	11	117038380	117038380	G	A	*PAFAH1B2*	nonsynonymous SNV	0.30303
C7-T	17	10352347	10352347	C	T	*MYH4*	nonsynonymous SNV	0.322034
C7-T	2	46607406	46607406	A	G	*EPAS1*	nonsynonymous SNV	0.287129
C7-T	18	61652416	61652416	C	G	*SERPINB8*	synonymous SNV	0.273684

* Mutations were described according to the hg19 reference genome.

Supplementary Table 3. Results of validation of *EPAS1* mutations.

Sample name	Sample type	Chr *	Start	End	Ref	Alt	Gene	Type of mutations	VAF in samples	Results of validation						
										Number of valiant reads in samples	Number of total reads in samples	VAF in samples	Number of valiant reads in controls	Number of total reads in controls	VAF in controls	Validation
C1-T1	FF	2	46607402	46607402	C	T	*EPAS1*	nonsynonymous SNV	0.247	421953	1607209	0.263	1216	2141818	0.001	Validated
C1-T2	FF	2	46607436	46607436	T	G	*EPAS1*	nonsynonymous SNV	0.282	533411	2111845	0.253	389	2142014	0.000	Validated
C1-T3	FF	2	46607405	46607405	T	A	*EPAS1*	nonsynonymous SNV	0.125	252962	1916516	0.132	918	2141651	0.000	Validated
C2-T1	FFPE	2	46607402	46607402	C	A	*EPAS1*	nonsynonymous SNV	0.337	733852	1821897	0.403	678	1830256	0.000	Validated
C2-T2	FFPE	2	46607427	46607427	A	C	*EPAS1*	nonsynonymous SNV	0.302	527627	1792552	0.294	1262	1827811	0.001	Validated
C2-T3	FFPE	2	46607400	46607400	C	T	*EPAS1*	nonsynonymous SNV	0.356	696826	2049302	0.340	1568	1831714	0.001	Validated
C2-T4	FF	2	46607402	46607402	C	T	*EPAS1*	nonsynonymous SNV	0.314	556601	1593926	0.349	1695	2938246	0.001	Validated
C2-T5	FF	2	46607409	46607409	T	A	*EPAS1*	nonsynonymous SNV	0.183	407897	2020396	0.202	2976	2934697	0.001	Validated
C2-T6	FF	2	46607399	46607399	G	C	*EPAS1*	nonsynonymous SNV	0.243	357131	1494777	0.239	6728	2935037	0.002	Validated
C3-T1	FFPE	2	46607410	46607410	C	G	*EPAS1*	nonsynonymous SNV	0.292	793345	2378054	0.334	410	1044454	0.000	Validated
C3-AMH	FFPE	2	46607403	46607403	C	T	*EPAS1*	nonsynonymous SNV	0.104	144891	1114045	0.130	1596	1044442	0.002	Validated
C4-T	FFPE	2	46607402	46607402	C	T	*EPAS1*	nonsynonymous SNV	0.270	326738	1224277	0.267	912	1176471	0.001	Validated
C5-T	FFPE	2	46607402	46607402	C	T	*EPAS1*	nonsynonymous SNV	0.373	457005	1039610	0.440	695	1130717	0.001	Validated
C6-T	FFPE	2	46607400	46607400	C	G	*EPAS1*	nonsynonymous SNV	0.297	468935	1182571	0.397	674	1044629	0.001	Validated
C7-T	FFPE	2	46607406	46607406	A	G	*EPAS1*	nonsynonymous SNV	0.287	255041	901891	0.283	353	935756	0.000	Validated

* Mutations were described according to the hg19 reference genome.

Supplementary Table 4. Clinical characteristics of patients with CCHD-PPGL as compared with non-CCHD-PPGL from the TCGA cohort.

Clinical characteristics	CCHD (n=7)	Non-CCHD-PPGL (n=165)	*P* value
Median age at initial diagnosis of PPGLs (range) -yr	26 (18-46)	46 (19-83)	1.5×10^{-3}
Female sex -no.(%)	4 (57)	92 (56)	1
Occurrence of PGL -no.(%)	6 (86)	28 (17)	2.4×10^{-4}
Bilateral adrenal PCC -no.(%)	0 (0)	10 (6)	1
Multiple PPGLs (excluding only bilateral PCC) -no.(%)	3 (43)	10 (6)	1.0×10^{-2}
Metastatic disease -no.(%)	1 (14)	11 (7)	0.4

PGL, extra-adrenal paraganglioma; PCC, pheochromocytoma.